Published in final edited form as:

Nature. 2018 November ; 563(7732): 569–573. doi:10.1038/s41586-018-0697-7.

Autophagy maintains tumor growth through circulating arginine

Laura Poillet-Perez[1], **Xiaoqi Xie**[1], **Le Zhan**[1], **Yang Yang**[1], **Daniel W. Sharp**[1], **Zhixian Sherrie Hu**[1], **Xiaoyang Su**[1,3], **Anurag Maganti**[1], **Cherry Jiang**[1], **Wenyun Lu**[4], **Haiyan Zheng**[2], **Marcus W. Bosenberg**[5], **Janice M. Mehnert**[1,6], **Jessie Yanxiang Guo**[1,3,7], **Edmund Lattime**[1,8], **Joshua D. Rabinowitz**[1,4], and **Eileen White**[1,9]

[1]Rutgers Cancer Institute of New Jersey, New Brunswick, NJ 08903 USA

[2]Biological Mass Spectrometry Facility, Rutgers University, Robert Wood Johnson Medical School, Rutgers University, Piscataway, NJ 08854 USA

[3]Department of Medicine, Robert Wood Johnson Medical School, Rutgers University, New Brunswick, NJ 08903 USA

[4]Department of Chemistry and Lewis-Sigler Institute for Integrative Genomics, Princeton University, Princeton, NJ 08544, USA

[5]Department of Pathology, Yale University School of Medicine, New Haven, Connecticut 06510 USA

[6]Department of Medicine, Division of Medical Oncology, Developmental Therapeutics Unit, Robert Wood Johnson Medical School, Rutgers University, New Brunswick, NJ 08903 USA

[7]Department of Chemical Biology, Rutgers Ernest Mario School of Pharmacy, Piscataway, NJ 08854 USA

[8]Department of Surgery, Robert Wood Johnson Medical School, Rutgers University, New Brunswick, NJ 08903 USA

[9]Department of Molecular Biology and Biochemistry, Rutgers University, Piscataway, NJ 08854 USA

Abstract

Correspondence and requests for materials should be addressed to E.W. (epwhite@cinj.rutgers.edu).

Author Contributions L.P.P. performed the majority of the experimental work and wrote the manuscript. L.Z. performed surgery and infusion with labelled-arginine. Y.Y developed the methods and provided the mice required for generating $Atg5^{\Delta/\Delta}$ and liver-specific $Atg5^{\Delta/\Delta}$ hosts. A.M and C.J assisted with *in vitro* experiments. X.X. and J.Y.G. performed some of the tumor growth experiments. J.M.M. provided melanoma expertise. D.W.S. and E.L. assisted with CD4/CD8 depletion. Z.S.H. assisted with mouse husbandry. H.Z. performed proteomics processing and analysis. X.S., W.L. and J.D.R. performed metabolomics processing and analysis. M.W.B. provided YUMM 1.1, 1.3, 1.7 and 1.9 melanoma cells. E.W. is the leading principal investigator who conceived the project, supervised research and edited the paper.

Supplementary Information is available in the online version of the paper.

Data availability. All data are available from the authors upon reasonable request. Source Data for Figs 1d, 2b, 3d are provided with the online version of the paper. The raw mass spectrometry data have been deposited in the MassIVE repository, entry MSV000082879.

The other authors declare no competing financial interests.

Autophagy captures intracellular components and delivers them to lysosomes where they are degraded and recycled to sustain metabolism and to enable survival in starvation[1–5]. Acute, whole-body deletion of the essential autophagy gene *Atg7* in adult mice causes a systemic metabolic defect manifested by starvation intolerance and gradual loss of white adipose tissue (WAT), liver glycogen, and muscle mass1. Cancer cells also benefit from autophagy. Deletion of essential autophagy genes impairs the metabolism, proliferation, survival and malignancy of spontaneous tumors in autochthonous cancer models[6,7]. Acute, systemic deletion of *Atg7* or acute, systemic expression of a dominant-negative ATG4b in mice induces greater regression of Kras-driven cancers than tumor-specific autophagy deletion, suggesting a role for host autophagy in promoting tumor growth[1,8]. Here we show that host-specific *Atg7* deletion impairs growth of multiple different allografted tumors, although not all tumor lines were sensitive to host autophagy status. Host autophagy loss was associated with reduction in circulating arginine and the sensitive tumor cells lines were arginine auxotrophs due to lack of expression of the enzyme argininosuccinate synthase (ASS1). Serum proteomic analysis identified the arginine-degrading enzyme Arginase I (ARG1) in the circulation of *Atg7*-deficient hosts, and *in vivo* arginine metabolic tracing demonstrated degradation of serum arginine to ornithine. ARG1 is predominantly expressed in liver and can be released from hepatocytes into the circulation. Liver-specific *Atg7* deletion produced circulating ARG1, and reduced serum arginine and tumor growth. Deletion of *Atg5* in the host similarly regulated circulating arginine and tumorigenesis, demonstrating specificity to autophagy function. Dietary supplementation of *Atg7*-deficient hosts with arginine partially restored circulating arginine levels and tumor growth. Thus, defective host autophagy leads to release of ARG1 from liver and degradation of circulating arginine essential for tumor growth, identifying a novel metabolic vulnerability of cancer.

To validate whether host autophagy promotes tumor growth, we tested the growth of an autophagy-competent C57Bl/6J isogenic $Braf^{V600E/+}$, $Pten^{-/-}$, $Cdkn2^{-/-}$ mouse melanoma cell line (YUMM 1.1) in C57Bl/6J host mice without ($Atg7^{+/+}$) and with ($Atg7^{\Delta/\Delta}$) conditional, whole body *Atg7* deficiency (Fig. 1a). YUMM 1.1 tumors were significantly smaller when grown on $Atg7^{\Delta/\Delta}$ compared to $Atg7^{+/+}$ hosts (Fig. 1b), demonstrating that host autophagy promoted tumor growth. Examination of additional autophagy-competent isogenic C57Bl/6J $Braf^{V600E/+}$, $Pten^{-/-}$, $Cdkn2^{-/-}$ YUMM 1.3 melanoma, carcinogen-induced MB49 urothelial carcinoma, and $Kras^{G12D/+}$, $p53^{-/-}$ 71.8 non-small-cell lung cancer cell lines revealed a similar requirement for host autophagy for tumor growth (Extended data Fig. 1a, c, e). The decreased tumor growth observed in $Atg7^{\Delta/\Delta}$ hosts was associated with decreased proliferation. In some tumor types, there was also increased apoptosis (Fig. 1c and Extended data Fig. 1b, d, f). Host autophagy was, however, not required for the growth of autophagy-competent isogenic C57Bl/6J $Braf^{V600E/+}$, $Pten^{-/-}$, $Cdkn2^{-/-}$ YUMM 1.7 and 1.9 melanoma cell lines (Extended data Fig. 2a-d), indicating that dependency on host autophagy is common, but there are tumor-specific adaptation mechanisms.

The melanoma cell lines dependent on host autophagy for tumor growth are derived from genetically engineered mouse models of cancer and thereby have a low mutation burden and neoantigen load and fail to provoke an efficient T-cell response[9]. Nonetheless, autophagy modulates a variety of immune mechanisms that could underlie defective tumor growth on

autophagy-deficient hosts. *Atg7*$^{\Delta/\Delta}$ hosts did not modify infiltration of YUMM 1.1 tumors with CD3, CD4 or CD8 positive cells (Extended data Fig. 2e). Depletion of CD4+ and CD8+ T-cells modestly increased tumor growth in *Atg7*$^{+/+}$ hosts but did not significantly rescue growth in *Atg7*$^{\Delta/\Delta}$ hosts (Extended data Fig. 2f). Thus, despite relative increased fraction of myeloid-derived suppressor cells and CD8+ T cells in *Atg7*$^{\Delta/\Delta}$ hosts (Extended data Fig. 2g), the decreased tumor growth on *Atg7*$^{\Delta/\Delta}$ hosts was not due to induction of an anti-tumor T-cell response.

Autophagy supports metabolism by recycling cargo to provide anabolic and catabolic substrates[6]. This metabolic recycling function of autophagy promotes mammalian survival during fasting[1–3], and tumor cell survival to nutrient limitation[4,10,11]. One major source of tumor nutrients is from the host blood supply. Accordingly, we tested whether circulating nutrients provided by host autophagy were required for tumor growth. Metabolite profiling of serum from *Atg7*$^{+/+}$ and *Atg7*$^{\Delta/\Delta}$ hosts identified 12 metabolites that were decreased and 7 that were increased with autophagy knockout (Fig. 1d, Supplementary Table 1 and 2). Serum arginine was strikingly downregulated in *Atg7*$^{\Delta/\Delta}$ compared to *Atg7*$^{+/+}$ hosts (−2.37 log2 fold change) (Fig. 1d), confirming previous results[1].

Arginine is a non-essential amino acid derived from the diet, *de novo* synthesis and protein turnover, and is important for mTOR activation[12], ammonia detoxification through the urea cycle, as well as the synthesis of proteins, creatine, polyamines and nitric oxide (NO)[13]. It is long known that some human cancers silence expression of *ASS1* resulting in arginine auxotrophy[14]. Without ASS1, cancer cells are unable to synthesize arginine from citrulline and are dependent on exogenous arginine[15,16]. *ASS1* silencing prevents consumption of aspartate by the urea cycle, increasing the availability of this amino acid, which is required for pyrimidine biosynthesis and can become limiting in hypoxia (Fig. 1e)[17,18]. These findings suggested that low circulating arginine may underlie defective tumor growth on autophagy-deficient hosts.

To determine their requirement for exogenous arginine, YUMM 1.1, 1.3, 1.7, 1.9, MB49 and 71.8 cells were tested for growth without and with arginine. Proliferation was blocked *in vitro* in complete medium with the sole absence of arginine, and this was not associated with cell death. Growth rates increased with increased percentage of arginine in the medium demonstrating arginine auxotrophy (Fig. 1f and Extended data Fig. 3a). YUMM 1.1 tumors were tested for lack expression of enzymes involved in arginine biosynthesis: ASS1, Argininosuccinate Lyase (ASL) that converts citrulline to arginine, and Ornithine Transcarbamylase (OTC) that converts ornithine to citrulline (Fig. 1e). As previously shown for melanoma[19,20], irrespective of use of *Atg7*$^{+/+}$ and *Atg7*$^{\Delta/\Delta}$ hosts, tumors lacked ASS1 and OTC expression explaining arginine auxotrophy (Fig. 1g). In contrast to tumors, both *Atg7*$^{+/+}$ and *Atg7*$^{\Delta/\Delta}$ hosts express ASS1, ASL or OTC in liver and kidney suggesting that they are capable of arginine synthesis (Extended data Fig. 3b). Consistent with the YUMM 1.1 and the literature, YUMM 1.7 tumors which grew on *Atg7*$^{\Delta/\Delta}$ hosts also lacked expression of ASS1 and OTC, suggesting a mechanism of intrinsic resistance independent of arginine auxotrophy in a subset of tumor cell lines (Extended data Fig. 3c).

To determine how circulating arginine is depleted in *Atg7*$^{\Delta/\Delta}$ hosts, we examined the serum proteome by nano LC-MS/MS, identifying 19 proteins which were downregulated and 32 which were upregulated upon loss of *Atg7* (Fig. 2a and Supplementary Table 3). Among proteins upregulated in *Atg7*$^{\Delta/\Delta}$ hosts serum was ARG1 (2.43 log2 fold change) (Fig. 2b). ARG1 is expressed in liver where it degrades arginine to ornithine. Appearance of ARG1 in serum without altered levels in liver in *Atg7*$^{\Delta/\Delta}$ hosts was confirmed by western blotting (Fig. 2c). Serum NO levels were not modified, suggesting that serum arginase did not alter the arginine availability for NO synthesis (Extended data Fig. 3d). Serum arginase activity *in vitro* was increased as shown by greater $^{13}C_6$-arginine degradation to $^{13}C_5$-ornithine in serum from *Atg7*$^{\Delta/\Delta}$ hosts (Extended data Fig. 4a). To determine how *Atg7* deficiency altered arginine metabolism *in vivo*, we infused *Atg7*$^{+/+}$ and *Atg7*$^{\Delta/\Delta}$ hosts with $^{13}C_6$-$^{15}N_4$-labeled arginine for 3h (Fig. 2d)[21]. To analyze ^{13}C and ^{15}N enrichment, serum was collected at different times during infusion, and tumors, kidney and liver were collected at the end of the infusion (3h). *Atg7*$^{\Delta/\Delta}$ host serum showed decreased arginine (^{12}C, $^{13}C_6{}^{15}N_4$ and $^{13}C_5{}^{15}N_2$) associated with increased ornithine (^{12}C and $^{13}C_5{}^{15}N_2$), indicating degradation of circulating arginine to ornithine (Fig. 2e and Extended data Fig. 4b). *Atg7*$^{\Delta/\Delta}$ host kidney showed decreased arginine levels with no change in ornithine or citrulline; no difference was observed in arginine, citrulline or ornithine levels in liver of *Atg7*$^{\Delta/\Delta}$ compared to *Atg7*$^{+/+}$ hosts (Extended data Fig. 4c-d). Tumors from *Atg7*$^{\Delta/\Delta}$ hosts also displayed decreased arginine (^{12}C, $^{13}C_6{}^{15}N_4$ and $^{13}C_5{}^{15}N_2$) and increased ornithine levels (^{12}C and $^{13}C_5{}^{15}N_2$) (Fig. 2f). These results confirm that in ASS1-deficient tumors dependent on exogenous arginine, arginine is depleted, consistent with insufficient circulating arginine in *Atg7*$^{\Delta/\Delta}$ hosts.

During inflammation, injury and liver disease, ARG1 is released from hepatocytes into the circulation leading to arginine depletion[22]. *Atg7*$^{\Delta/\Delta}$ hosts have steatosis[1] and liver-specific deletion of *Atg5* or *Atg7* is associated with liver damage[2,23,24]. Accordingly, we hypothesized that ARG1 is released into the circulation following deletion of *Atg7* in liver. To test this hypothesis, we deleted *Atg7* specifically in the liver and examined arginine and ARG1 levels in the circulation, and tumor growth (Fig. 3a). Injection of AAV-TBG-iCre vector efficiently deleted *Atg7* in liver but not in others organs such as brain and kidney (Extended data Fig. 5a-c). As expected, liver-specific *Atg7* deletion led to histopathologic changes in liver cells without affecting other tissues (Extended data Fig. 5d). As seen in *Atg7*$^{\Delta/\Delta}$ hosts, liver-specific *Atg7*$^{\Delta/\Delta}$ hosts showed increased serum ARG1 (Fig. 3b), with reduced arginine and increased ornithine (Fig. 3c) and no change in NO levels (Extended data Fig. 5e). Liver-specific *Atg7* deletion also modified levels of other circulating metabolites, with 18 increased and 4 decreased in liver-specific *Atg7*$^{\Delta/\Delta}$ compared to *Atg7*$^{+/+}$ hosts (Supplementary Table 4 and 5). Some of these circulating metabolites (e.g. 4-pyridoxic acid, D-gluconate and glucuronic acid) were also altered in *Atg7*$^{\Delta/\Delta}$ hosts suggesting that their dysregulation had a liver-specific origin (Fig. 1d and Extended data Fig. 5f). Serum arginine was downregulated in liver-specific *Atg7*$^{\Delta/\Delta}$ compared to *Atg7*$^{+/+}$ hosts (Fig. 3d) as previously shown in *Atg7*$^{\Delta/\Delta}$ hosts (Fig. 1d). The weight and volume of melanoma tumors (YUMM 1.1) were significantly decreased in liver-specific *Atg7*$^{\Delta/\Delta}$ compared to *Atg7*$^{+/+}$ hosts (Fig. 3e), which was associated with decreased proliferation and no change in apoptosis (Fig. 3f). Tumors from liver-specific *Atg7*$^{\Delta/\Delta}$ hosts had decreased

arginine and increased ornithine, but to a lesser extent than the tumors from *Atg7*$^{\Delta/\Delta}$ hosts, which may explain why the decreased tumor growth in liver-specific *Atg7*$^{\Delta/\Delta}$ hosts was not as dramatic as with *Atg7*$^{\Delta/\Delta}$ hosts (Fig. 3g). In liver-specific *Atg7*$^{\Delta/\Delta}$ hosts, autophagy in the microenvironment may locally feed the tumor with amino acids, as previously shown in pancreatic cancer and in *Drosophila* tumors[25,26]. These results suggest that *Atg7* deletion in the liver is responsible for ARG1 release into the circulation leading to depletion of circulating arginine and decreased tumor growth.

To determine if the degradation of circulating arginine by ARG1 in *Atg7*$^{\Delta/\Delta}$ hosts was due to loss of autophagy, we examined mice with conditional deletion of *Atg5*. Whole-body conditional deletion of *Atg5* also introduced ARG1 into the circulation and decreased serum arginine, and tumor growth was also decreased on these *Atg5*$^{\Delta/\Delta}$ hosts (Extended data Fig. 6). Similar to liver-specific deletion of *Atg7*, liver-specific deletion of *Atg5* led to histopathologic liver changes with increased circulating ARG1 and reduced arginine (Extended data Fig. 7), confirming that modulation of circulating arginine and tumorigenesis was autophagy-dependent.

We next tested whether dietary arginine supplementation can rescue tumor growth in *Atg7*$^{\Delta/\Delta}$ hosts (Fig. 4a). Dietary arginine supplementation was able to partially increase serum arginine levels in *Atg7*$^{\Delta/\Delta}$ hosts and did not modify ornithine or citrulline levels (Fig. 4b). This increased circulating arginine promoted growth and proliferation of melanoma cell lines YUMM 1.1 and 1.3 in *Atg7*$^{\Delta/\Delta}$ compared to *Atg7*$^{+/+}$ hosts (Fig. 4c-d and Extended data Fig. 8a-c), confirming that limiting circulating arginine can curtail tumor growth.

In summary, autophagy in the liver prevents the release of ARG1 and the degradation of circulating arginine important for the growth of arginine auxotrophic tumors (Fig. 4e). As some tumor cells auxotrophic for arginine *in vitro* were capable of growth on *Atg7*$^{\Delta/\Delta}$ hosts, this suggests the existence of adaptation mechanisms[27]. Recent work demonstrated that autophagy in the local tumor microenvironment can provide amino acids that promote tumor growth[25,26]. Our work demonstrates that host autophagy also sustains a circulating amino acid (arginine) essential for tumor growth. This finding underscores the importance of understanding the sensitivity of ASS1-deficient tumors to arginine deprivation therapy[28] with or without autophagy inhibition[29]. As tumor nutrients are mainly derived from the host circulation, restricting essential tumor nutrients in the circulation, as done with asparaginase treatment, is a form of cancer therapy ripe to be exploited further[30].

METHODS

Mice.

All animal care and treatments were carried out in compliance with Rutgers University Institutional Animal Care and Use Committee guidelines (IACUC). Mice for conditional whole-body *Atg7* deletion (C57Bl/6J Ubc-*Cre*$^{ERT2/+}$;*Atg7*$^{flox/flox}$) were engineered with floxed alleles of *Atg7* (*Atg7*$^{flox/flox}$)[2] and a transgene expressing the Tamoxifen (TAM)-regulated Cre recombinase fusion protein under the control of the ubiquitously expressed ubiquitin C promoter (Ubc)[31] as previously described[1]. Acute deletion of *Atg7* throughout the mouse is obtained after TAM injection[1]. TAM (T5648, Sigma) was suspended at a

concentration of 20 mg/ml, in a mixture of 98% sunflower seed oil and 2% ethanol and 200 µl per 25 g of body weight was injected intraperitoneally into 8 to 10 weeks old male Ubc-*Cre*$^{ERT2/+}$;*Atg7*$^{+/+}$ or Ubc-*Cre*$^{ERT2/+}$;*Atg7*$^{flox/flox}$ mice once per day for 4 days to generate cohorts of *Atg7* deleted (*Atg7*$^{\Delta/\Delta}$) and wild type (*Atg7*$^{+/+}$) control host mice. To assess the consequence of acute *Atg7* deletion on tumorigenesis of C57Bl/6J isogenic male tumor cells, one week post TAM treatment, YUMM 1.1 (1×10^6 cells), 1.3 (2×10^6 cells), 1.7 (0.1×10^6 cells), 1.9 (1×10^6 cells), 71.8 (1×10^6 cells) or MB49 (0.25×10^6 cells) cells were resuspended in 100 µL PBS and injected subcutaneously into the dorsal flanks of mice. Three weeks post cell injection, mice were sacrificed and serum and tumors were collected. The maximal tumor volume (1700 mm^3) permitted by Rutgers University IACUC was never exceeded. For arginine supplementation, 1% arginine (A8094, Sigma) in drinking water was given to the mice a week before TAM and throughout the experiment.

Mice for conditional whole-body *Atg5* deletion (C57Bl/6J Ubc-*Cre*$^{ERT2/+}$;*Atg5*$^{flox/flox}$) were engineered with floxed alleles of *Atg5* (*Atg5*$^{flox/flox}$)[32] and a transgene expressing the Tamoxifen (TAM)-regulated Cre recombinase fusion protein under the control of the ubiquitously expressed ubiquitin C promoter (Ubc)[31]. Acute deletion of *Atg5* throughout mice was obtained after TAM injection (200 µl of TAM per 25 g of body weight injected intraperitoneally into 8 to 10 week old male Ubc-*Cre*$^{ERT2/+}$;*Atg5*$^{+/+}$ or Ubc-*Cre*$^{ERT2/+}$;*Atg5*$^{flox/flox}$ mice once a week for 4 weeks) to generate cohorts of *Atg5* deleted (*Atg5*$^{\Delta/\Delta}$) and wild type (*Atg5*$^{+/+}$) control host mice.

Liver-specific *Atg7* and *Atg5* deletion was achieved by injected an Adeno Associated Virus (AAV)-thyroxine binding globulin (TBG) promoter-Cre recombinase vector (AAV-TBG-iCre, Vector Biolabs) to *Atg7*$^{flox/flox}$ and *Atg5*$^{flox/flox}$ mice. An AAV-TBG promoter-GFP vector (AAV-TBG-GFP, Vector Biolabs) was injected to *Atg7*$^{flox/flox}$ and *Atg5*$^{flox/flox}$ mice as a control. 1.5×10^{11} genome copy (g.c) of either AAV-TBG-iCre or AAV-TBG-GFP vectors in 100µl PBS was injected into the tail vein of 8 to 10 week old male *Atg7*$^{flox/flox}$ and *Atg5*$^{flox/flox}$ mice to generate liver-specific *Atg7*$^{\Delta/\Delta}$ or *Atg5*$^{\Delta/\Delta}$ and *Atg7*$^{+/+}$ or *Atg5*$^{+/+}$ control mice, respectively. Three weeks post injection, YUMM 1.1 cells (1×10^6 cells) were resuspended in 100 µL PBS and injected subcutaneously into the dorsal flanks of the liver-specific *Atg7*$^{\Delta/\Delta}$ and *Atg7*$^{+/+}$ control mice. Tumor growth was monitored daily. Tumor volume was calculated with the following formula: volume = π/6 x L x W x H. Three weeks post cell injection, mice were sacrificed and liver, kidney, brain, serum and tumors were collected.

Cell lines.

Cell culture.—Cell lines were authenticated using whole exome sequencing. YUMM 1.1, 1.3, 1.7 and 1.9 cells derived from *Braf*$^{V600E/+}$, *Pten*$^{-/-}$, *Cdkn2*$^{-/-}$ C57Bl/6J mouse melanomas were generated previously[33] and cultured in Dulbecco's minimum essential medium and Ham's F12 (DMEM-F12) (10–092-CV, Corning) supplemented with 10% fetal bovine serum (FBS) (F0926, Sigma) in a 5% CO_2 incubator at 37°C. Mouse lung cancer cell line 71.8 was derived from *p53*$^{-/-}$, *Kras*$^{G12D/+}$ mouse lung tumors previously[11] and the MB49 cell line[34] was provided by the Ratliff laboratory and cultured in Roswell Park

Memorial Institute medium (RPMI) (11875–093, Gibco). Cells were tested negative for mycoplasma contamination.

Cell proliferation in arginine-deficient medium.—YUMM 1.1, 1.3, 1.7, 1.9, 71.8 and MB49 cell were seeded at a density of 15,000 cells per well in 24-well plates. The following day, cells were washed with phosphate-buffered saline (PBS) (14190–144, Gibco) and cultured in arginine-free DMEM-F12 (DFL27, Caisson Labs) or arginine-free RPMI (R1780, Sigma) supplemented with 10% dialyzed FBS (89986, Thermo Scientific) and an increasing percentage of arginine from 2.5 to 100%. Growth was assessed using an IncuCyte ZOOM™ with images of the proliferative cells recorded every 2 hours for a total duration of 6 days.

Metabolite analysis by LC-MS.

Metabolite extraction for LC-MS.—Metabolites from 10 μl serum samples were first extracted with 40 μl of ice-cold methanol. The mixture was allowed to sit at −20°C for 20 min, and then centrifuged at 16,000×g for 10 min at 4°C. Supernatants were transferred to clean tubes and pellets were extracted again with 200 μl 40:40:20 methanol:acetonitrile:H_2O. The mixture was allowed to sit on ice for 10 min, and then centrifuged at 16,000×g for 10 min at 4°C. Supernatants were combined with the first extraction, resulting in roughly 240 μl of extract. Extracts were further processed with Phree® Phospholipid Removal 1mL Tube (Phenomenex) according to the manufacturer's instructions. The final extract was stored at −80°C until analyzed by LC-MS. To extract metabolites from the tissues and tumors, samples (25 mg) were first pulverized using a Cryomill (Retsch) in liquid nitrogen at 25Hz for 2 min. Extraction was performed by adding −20°C 40:40:20 methanol:acetonitrile:water with 0.5% formic acid solution (500 μl) to the ground samples, followed by vortexing and centrifugation at 16,000×g for 10 min at 4°C. The supernatants were transferred to clean tubes and the pellets were extracted again by repeating the previous step. The supernatant was then combined with the first extract. 500 μl of extract was neutralized with 44 μl of 15% NH_4HCO_3 solution and centrifuged at 16,000×g for 10 min at 4°C to remove protein precipitate. 300 μl of supernatant was removed to clean tubes and stored at −80°C until analyzed by LC-MS.

LC-MS analysis.—LC−MS analysis of the extracted metabolites was performed on a Q Exactive PLUS hybrid quadrupole-orbitrap mass spectrometer (ThermoFisher Scientific) coupled to hydrophilic interaction chromatography (HILIC). The LC separation was performed on UltiMate 3000 UHPLC system with an XBridge BEH Amide column (150 mm × 2.1 mm, 2.5 μM particle size, Waters) with the corresponding XP VanGuard Cartridge. The liquid chromatography used a gradient of solvent A (95%:5% H_2O:acetonitrile with 20mM ammonium acetate, 20mM ammonium hydroxide, pH 9.4), and solvent B (20%:80% H_2O:acetonitrile with 20 mM ammonium acetate, 20 mM ammonium hydroxide, pH 9.4). The gradient was 0 min, 100% B; 3 min, 100% B; 3.2 min, 90% B; 6.2 min, 90% B; 6.5 min, 80% B; 10.5 min, 80% B; 10.7 min, 70% B; 13.5 min, 70% B; 13.7 min, 45% B; 16 min, 45% B; 16.5 min, 100% B. The flow rate was 300 μl/min. Injection volume was 5 μl and column temperature 25°C. The MS scans were in negative ion mode with a resolution of 70,000 at m/z 200. The automatic gain control (AGC) target was 3×10^6

and the scan range was 75−1000. In order to increase metabolome coverage, the samples were also analyzed with a secondary LC-MS method, which involves two separate instrument platforms covering both positive charged and negative charged metabolites. Negative charged metabolites were analyzed via reverse-phase ion-pairing chromatography coupled to an Exactive orbitrap mass spectrometer (ThermoFisher Scientific). The mass spectrometer was operated in negative ion mode with resolving power of 100,000 at m/z 200, scanning range being m/z 75–1000. The LC method has been described previously[35], using a Synergy Hydro-RP column (100 mm × 2 mm, 2.5 μm particle size, Phenomenex) with a flow rate of 200 μL/min. The LC gradient was 0 min, 0% B; 2.5 min, 0% B; 5 min, 20% B; 7.5 min, 20% B; 13 min, 55% B; 15.5 min, 95% B; 18.5 min, 95% B; 19 min, 0% B; 25 min, 0% B. Solvent A is 97:3 water:methanol with 10 mM tributylamine and 15 mM acetic acid; solvent B is methanol. Positive charged metabolites were analyzed on a Q Exactive Plus mass spectrometer coupled to Vanquish UHPLC system (ThermoFisher Scientific). The mass spectrometer was operated in positive ion mode with resolving power of 140,000 at m/z 200, scanning range being m/z 75– 1000. The LC separation was achieved on an Agilent Poroshell 120 Bonus-RP column (150 × 2.1 mm, 2.7 μm particle size). The gradient was 0 min, 50 μL/min, 0.0%B; 6 min, 50 μL/min, 0% B; 12 min, 200 μL/min, 70% B; 14 min, 200 μL/min, 100 %B; 18 min, 200 μL/min, 100% B; 19 min, 200 μL/min, 0% B; 24 min, 200 μL/min, 0% B; 25 min, 50 μL/min, 0% B. Solvent A is 10mM ammonium acetate + 0.1% acetic acid in 98:2 water:acetonitrile and solvent B is acetonitrile[36]. Metabolite features were extracted in MAVEN v707[37] with the labeled isotope specified and a mass accuracy window of 5 ppm. For the ^{13}C-^{15}N arginine infusions, the isotope natural abundance and impurity of labeled substrate was corrected using a matrix-based algorithm.

Labelled arginine infusion.

For jugular vein catheterization, the procedure was modified from work previously described[38]. In brief, *Atg7*$^{\Delta/\Delta}$ and *Atg7*$^{+/+}$ mice were anesthetized using isoflurane carried by oxygen, followed by placement of a central venous catheter (polyurethane tubing, 1F in O.D.) (SAI Infusion Technologies) into the right jugular vein. A minimal amount of blood was carefully withdrawn to verify the catheter patency. Afterwards, the saline solution in the catheter was replaced by heparin/glycerol catheter lock solution (SAI Infusion Technologies). The proximal end of the catheter was then tunneled subcutaneously, exited between the shoulder blades, and properly secured. A fully recovered surgical mouse was placed in a plastic harness (SAI Infusion Technologies), and the catheter was connected to an infusion pump (New Era Pump System, Inc) through a mouse tether and swivel system (Instech Laboratories). Arginine isotope tracer ($^{13}C_6{}^{15}N_4$, CNLM-539-H-PK, Cambridge Isotope Laboratories) was dissolved in sterile saline and infused at a rate of 3.5 nmol/g/min (0.1 μl/g/min) for 3 hours. Infusion rate was determined using turnover flux calculations[21]. Mice were sacrificed after infusion for serum, tumor, liver and kidney analysis by LC-MS. The isotope natural abundance and impurity of labeled substrate was corrected using a matrix-based algorithm. The construction of the purity matrix and C/N joint correction matrix is similar to AccuCor[39]. For calculation of the circulating amino acid concentration, the average ion counts from the *Atg7*$^{+/+}$ mice were normalized to the amino acid concentration measured previously[40]. The amino acid concentration in the *Atg7*$^{\Delta/\Delta}$ mice were calculated proportionally.

Arginase activity assay.

To follow conversion of arginine to ornithine, 15 μl serum samples were added to 5 μl of 9.7 mM $MnCl_2$, 5 μl of 360 mM pH 9.7 glycine and 5 μl of 300 μM $^{13}C_6$-arginine followed by incubation at 37°C for 0, 5, 20, 60 or 120 min. 870 μl 40:40:20 methanol:acetonitrile:water with 0.5% formic acid solution were added to stop the reaction; the mixture was allowed to sit on ice for 10 min. The extract was neutralized with 40 μl of 15% NH_4HCO_3 solution and centrifuged at 16,000×g for 10 min at 4°C. 500 μl of supernatant was removed to clean tubes and stored at −80°C until analyzed by LC-MS. The LC−MS analysis was performed on the Q Exactive PLUS mass spectrometer coupled to UltiMate 3000 UHPLC system with an XBridge BEH Amide column (150 mm × 2.1 mm, 2.5 μM particle size, Waters, Milford, MA) with the corresponding XP VanGuard Cartridge. The liquid chromatography used a 6-min isocratic elution of 28% solvent A (95%:5% H_2O:acetonitrile with 20mM ammonium acetate, 20 mM ammonium hydroxide, pH 9.4) and 72% solvent B (20%:80% H_2O:acetonitrile with 20 mM ammonium acetate, 20 mM ammonium hydroxide, pH 9.4). The flow rate was 300 μl/min. Injection volume was 5 μl and column temperature 25°C. The MS scans were in negative ion mode with a resolution of 70,000 at m/z 200. The automatic gain control (AGC) target was 3×10^6 and the scan range was 75−1000. Metabolite features were extracted in MAVEN v707 with the labeled isotope specified and a mass accuracy window of 5 ppm.

Proteomic Analysis by LC-MS.

Technical duplicate of pooled serum samples from both *Atg7*$^{+/+}$ (n=5) and *Atg7*$^{\Delta/\Delta}$ (n=5) mice were processed in parallel. Two different methods were also used to reduce the amount of the major serum proteins to allow detection of rarer components: AlbuVoid™ (Biotech Support Group, LLC) was used to deplete albumin while the Agilent multiple affinity removal spin cartridge mouse 3 system (Mars3) was used to remove albumin, IgG, and transferrin following the manufacturer's protocol. Untreated or depleted sera were loaded onto NuPage™ 10% Bis-Tris Gel (Invitrogen), run a short distance into the gel, and proteins reduced, alkylated and digested with trypsin as described[41]. Digests were analyzed by nano LC-MS/MS using a Dionex Ultimate 3000 RLSC nano System interfaced with Q Exactive HF (Thermofisher). Peptides were loaded onto a self-packed 100 μm x 2 cm trap (Magic C18AQ, 5 μm 200 Å, Michrom Bio resources, Inc.) and washed with Buffer A (0.1% trifluoroacetic acid) for 5 min with a flow rate of 10 μl/min. The trap was brought in-line with the analytical column (self-packed Magic C18AQ, 3 μm 200 Å, 75 μm x 50 cm) and fractionated at 300 nl/min using a segmented linear gradient of 4–15% B in 30 min (A: 0.2% formic acid; B: 0.16% formic acid/80% acetonitrile), 15–25%B in 40min, 25–50% in 44 min and 50–90%B in 11 min. Mass spectrometry data was acquired using a data-dependent acquisition procedure with each cycle consisting of a MS1 scan (resolution 120,000) followed MS/MS scans (HCD relative collision energy 27%, resolution 30,000) of the 20 most intense ions using a dynamic exclusion duration of 20 sec. The raw data was converted into MASCOT Generic Format (MGF) using Proteome Discover 2.1 (ThermoFisher) and searched against the Ensemble mouse database and a database of common laboratory contaminants (http://www.thegpm.org/crap/) using a local implementation of the global proteome machine (GPM Fury)[42]. Peptide spectrum matches were assigned to genes using BioMart Ensembl tables. To estimate differential abundances of proteins, data from all LC-

MS runs were combined (neat, Albivoid-depleted, and Mars3-depleted for each of the four samples). For mouse proteins having 10 or more spectral counts, differential expression was estimated using the QLSpline option of the QuasiSeq package (https://cran.r-project.org/web/packages/QuasiSeq/index.html)43. Data is presented as thresholded log2 fold change of $Atg7^{\Delta/\Delta}/Atg7^{+/+}$ with adjusted p-values <0.05. p-values were adjusted using Holm correction using the "p.adjust" function in the base R package (https://cran.r-project.org). The raw mass spectrometry data have been deposited in the MassIVE repository, entry MSV000082879.

Enzymatic assays.

Serum nitric oxide levels were determined with the nitric oxide assay kit (ab65328, Abcam).

Histology.

Mouse tissues were fixed in 10% buffer formalin solution overnight and then transferred to 70% ethanol for paraffin-embedded sections. Tissue sections were deparaffinized, rehydrated and boiled for 45 min in 10 mM pH 6 Citrate buffer. Slides were blocked in 10% goat serum for an hour and then incubated at 4˚C overnight with primary antibody against Ki67 (1:200, Ab15580, Abcam), active Caspase-3 (1:300, #9661, Cell Signaling), CD3 (1:100, Ab16669, Abcam), CD4 (1:1,000, Ab183685, Abcam) and CD8 (1:100, 14–0808-82, Invitrogen). The following day, tissue sections were incubated with biotin-conjugated secondary antibody for 15min (Vector Laboratories), 3% hydrogen peroxide for 5 min, horseradish peroxidase streptavidin for 15 min (SA-5704, Vector Laboratories) and developed by 3,3-diaminobenzidine (Vector Laboratories) followed by hematoxylin staining (3536–16, Ricca). Sections were then dehydrated, mounted in Cytoseal 60 mounting medium (8310, Thermo Scientific) and analyzed using Nikon Eclipse 80i microscope. For quantification of IHC, at least 10 images containing a minimum of 100 cells were analyzed at 60X magnification for each genotype.

Western Blotting.

Tissues and tumor samples were grounded in liquid nitrogen, lysed in Tris lysis buffer (50 mM Tris HCl, 150 mM NaCl, 1 mM EDTA, 0.1% NP40, 5 mM MgCl2, 10% glycerol), separated on 12.5% SDS-PAGE gel and then transferred on PVDF membrane (Millipore). Membranes were blocked with 5% non-fat milk for 1 hour and probed overnight at 4˚C with antibodies against ASS1 (1:1,000, Ab170952, Abcam), ASL (1:500, sc-374353, Santa Cruz), OTC (1:500, sc-515791, Santa Cruz), ARG1 (1:500, sc-271430, Santa Cruz), ATG7 (1:2,000, A2856, Sigma), transferrin (1:1,000, sc-22597, Santa Cruz), ATG5 (1:1,500, Ab108327, Abcam) and β-actin (1:5,000, A1978, Sigma). Immunoreactive bands were detected using peroxidase-conjugated antibody (GE Healthcare) and enhanced chemiluminescence detection reagents (NEL105001EA, Perkin Elmer) and were analyzed using the ChemiDoc XRS+ system (Biorad). Protein levels were quantified using the Image Lab v6.0.1 software. Antibodies were validated with the use of positive and negative control following manufacturer's protocol.

T cell depletion and flow cytometry.

A week post TAM and every 5 days, 200 μg of CD4 (clone GK1.5; BE003–1, BioXCell) and CD8 (clone 2.43; BE0061, BioXCell) antibodies were injected intraperitoneally into $Atg7^{\Delta/\Delta}$ and $Atg7^{+/+}$ mice. Two days after the first antibody injection, YUMM 1.1 (1×10^6 cells) cells were resuspended in 100 mL PBS and injected subcutaneously into the dorsal flanks of the mice. Three weeks post cell injection, mice were sacrificed and tumors and spleen were collected. Tumors were homogenized in PBS in a gentleMACS Octo Dissociator (Miltenyi Biotec Inc.) according to manufacturer's protocol, and passed through a 70 mm cell restrainer. Spleens were grounded with a rubber grinder through steel mesh, treated with ACK Lysis Buffer to remove erythrocytes and passed through a 70 mm cell restrainer. Nonspecific binding of antibodies to cell Fc receptors was blocked using 20 mL/10^7 cells of FcR blocker (Miltenyi Biotec Inc). Cell surface immunostaining was performed with the following antibodies (1:200) : CD11c-PE-eFluor610 (clone N418, 61–0114-82), CD4-APC (clone GK1.5, 17–0041-82) CD3-AF700 (clone 17A2, 56–0032-82) and CD11b-APC-Cy7 (clone M1/70, A15390) (eBioscience); and CD45-FITC (clone 30-F11, 103107), MHC-II-BV605 (clone M5/114.15.2, 107639), Ly6G-BV650 (clone 1A8, 127641) and CD8-BV785 (clone 53.67, 100749) (BioLegend). Aqua Live/Dead (Invitrogen) was included to determine live cells. After staining of surface markers, cells were fixed and permeabilized using Transcription Factor staining kit and stained with FoxP3-eFluor450 (eBioscience). Cell staining data were acquired using a LSR-II flow cytometer (BD Biosciences, BD FACS Diva v2 software) and analyzed with FlowJo v10 software (Tree Star). Live lymphocytes were gated using forward scatter area (FSC-A) versus side scatter area (SSC-A), followed by FSC-A versus forward scatter height (FSC-H), SSC-A versus side scatter height (SSC-H) plots, forward scatter width (FSC-W) versus side scatter width (SSC-W), and Aqua Live/Dead. Populations were gated as follows: CD45 (%CD45+ of total live lymphocytes), CD3 (%CD3+ of CD11b-, CD11c-, CD45+), CD8 (%CD8+ of CD3), CD4 (%CD4+ of CD3), Treg (%FoxP3+ of CD4), DC (%CD11c+ of MHC-II+, CD45+), MDSC (%Ly6G, CD11b+ of MHC-II-, CD45+).

Antibodies for western blotting, flow cytometry and immunohistochemistry were validated with the use of positive and negative control (gene knock-outs and through the use of control tissues and cell lines) and following manufacturer's protocol.

Statistics.

All statistical analyses were performed with Prism v7 software using two-sided Student's *t*-test, unless specified otherwise. The sample size was chosen in advance on the basis of common practice of the described experiment and is mentioned for each experiment. No statistical methods were used to predetermine sample size. Each experiment was conducted with biological replicates and repeated multiple times. All attempts at replication were successful and no data were excluded. Mice were randomly allocated to experimental groups and the investigators were not blinded during the experiments and outcome assessment.

Extended Data

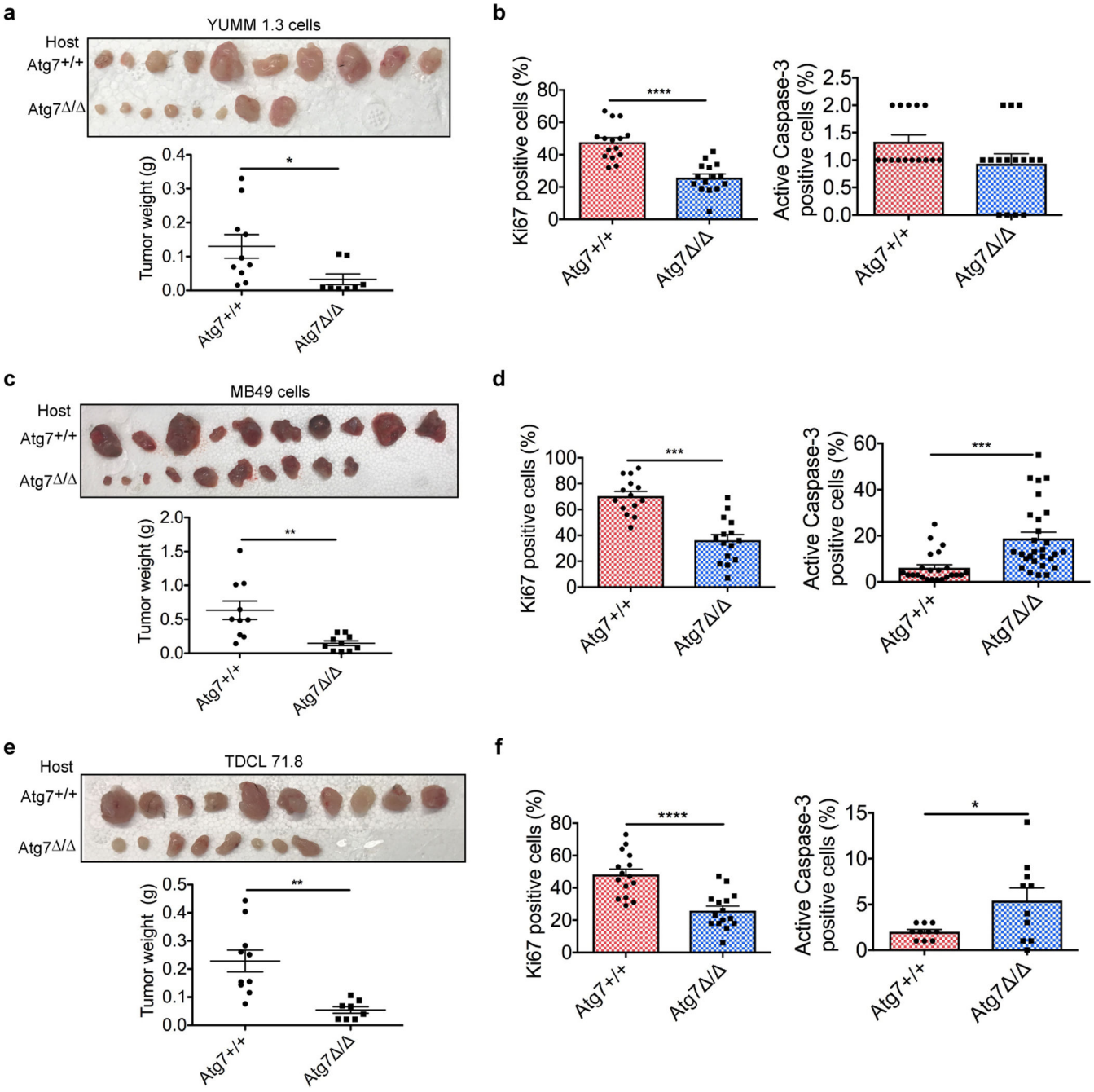

Extended data Fig. 1: Host autophagy promotes growth of different tumor cell types.

a-c-e, Comparison of tumor weight between *Atg7*$^{+/+}$ (n=5) and *Atg7*$^{\Delta/\Delta}$ **(a,** n=4; **c,** n=5; **e,** n=4) hosts after injection of 1.3 **(a)**, MB49 **(c)** or 71.8 **(e)** cells. Data are mean +/− S.E.M (*p<0.05, **p<0.01. **b-d-f,** IHC quantification of Ki67 and active Caspase-3 positive cells in tumors from *Atg7*$^{+/+}$ and *Atg7*$^{\Delta/\Delta}$ hosts. Data are mean +/− S.E.M (*p<0.05, ***p<0.001, ****p<0.0001).

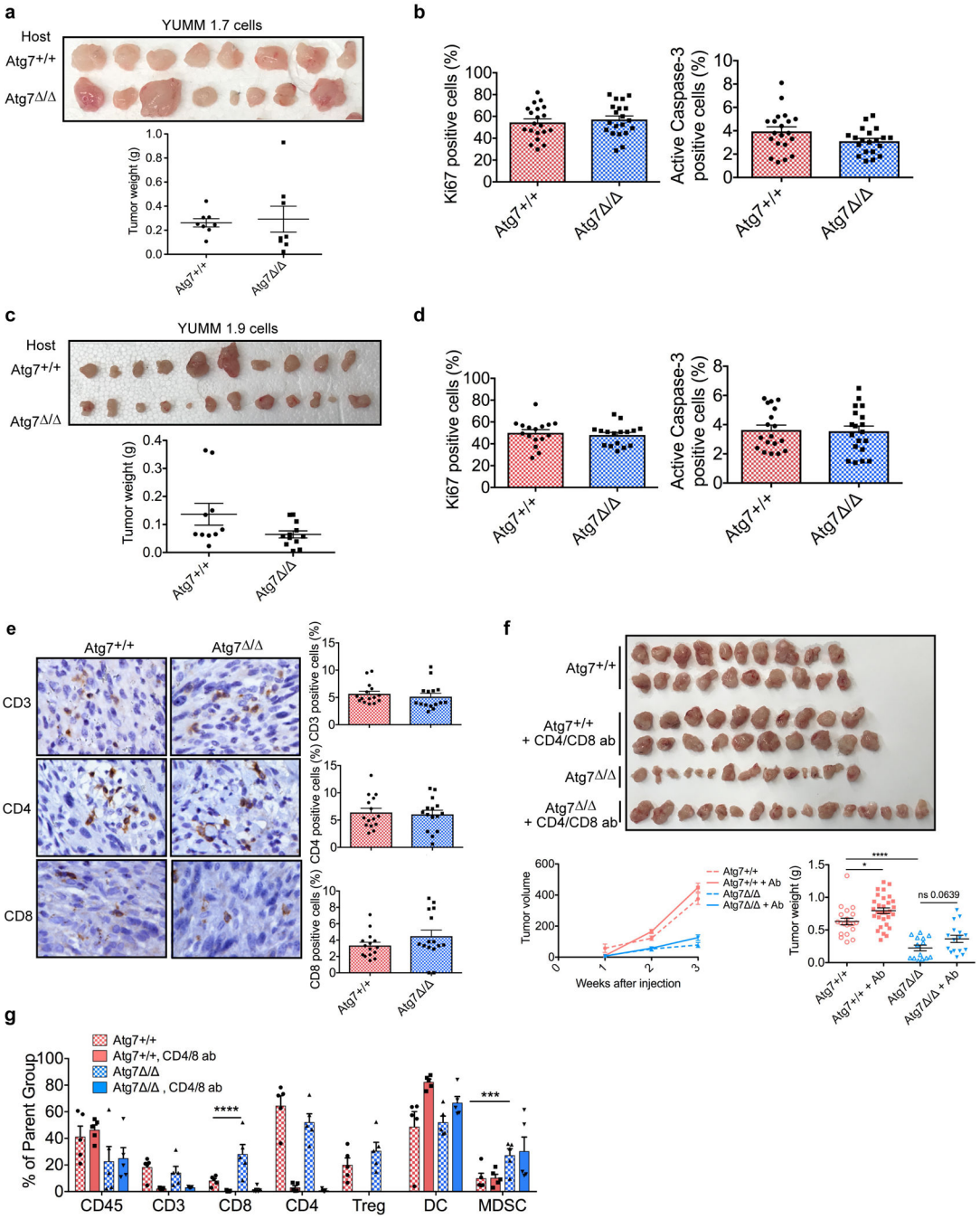

Extended data Fig. 2: Immune response is not involved in decreased tumor growth observed in *Atg7*$^{\Delta/\Delta}$ hosts.

a-c, Comparison of tumor weight between *Atg7*$^{+/+}$ (n=5) and *Atg7*$^{\Delta/\Delta}$ (**a,** n=5; **c,** n=6) hosts after injection of 1.7 **(a)**, 1.9 **(c)** cells. Data are mean +/− S.E.M. **b-d,** IHC quantification of Ki67 and active Caspase-3 positive cells in 1.7 **(b)** and 1.9 **(d)** tumors from *Atg7*$^{+/+}$ and *Atg7*$^{\Delta/\Delta}$ hosts. Data are mean +/− S.E.M. **e,** Representative IHC pictures and quantification of CD3, CD4 and CD8 positive cells in tumors from *Atg7*$^{+/+}$ and *Atg7*$^{\Delta/\Delta}$ hosts. Data are mean +/− S.E.M. **f,** Comparison of tumor volume and weight between *Atg7*$^{+/+}$ (n=10),

Atg7$^{+/+}$ + CD4/CD8 antibody depletion (n=15), *Atg7*$^{\Delta/\Delta}$ (n=7) and *Atg7*$^{\Delta/\Delta}$ + CD4/CD8 antibody depletion (n=8) hosts. Data are mean +/− S.E.M (*p<0.05, ****p<0.0001). **g,** Immune components fold change between *Atg7*$^{+/+}$ and *Atg7*$^{\Delta/\Delta}$ with or without antibody depletion (n=5 each). Treg, T regulatory cells; DC, dendritic cells; MDSC, myeloid-derived suppressor cells. Data are mean +/− S.E.M (***p<0.001, ****p<0.0001) by Two-way ANOVA test.

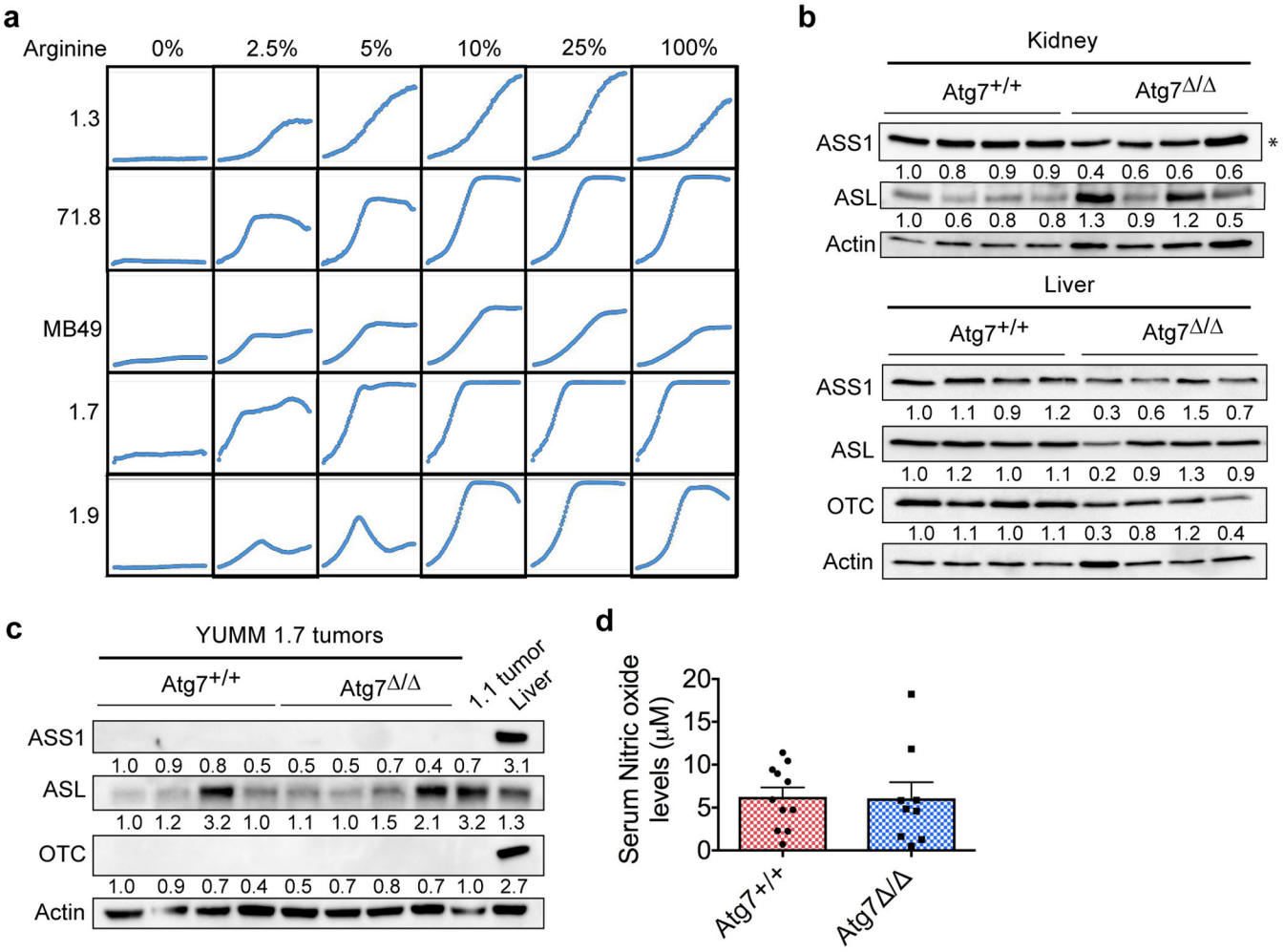

Extended data Fig. 3: Tumor cells are arginine auxotrophs.

a, YUMM 1.3, 71.8, MB49 and YUMM 1.7, 1.9 proliferation *in vitro* in medium containing different percentage of arginine. Cell density was measured every 2 hours using the IncuCyte. Data are representative of 3 independent experiments performed in duplicate. **b,** Western blotting showing expression of ASS1, ASL and OTC in kidney and liver from *Atg7*$^{+/+}$ and *Atg7*$^{\Delta/\Delta}$ hosts. *p<0.05 compared to *Atg7*$^{+/+}$ hosts. Data are representative of 3 independent experiments. Actin was used as a loading (Kidney ASL, Liver OTC) and processing (Kidney ASS1, Liver ASS1 and ASL) control. **c,** Western blotting showing expression of ASS1, ASL and OTC in YUMM 1.7 tumors from *Atg7*$^{+/+}$ and *Atg7*$^{\Delta/\Delta}$ hosts. Data are representative of 2 independent experiments. Actin was used as a loading (OTC)

and processing (ASS1, ASL) control. **d,** Analysis of serum nitric oxide levels in *Atg7*$^{+/+}$ (n=11) and *Atg7*$^{\Delta/\Delta}$ (n=9) hosts. Data are mean +/− S.E.M.

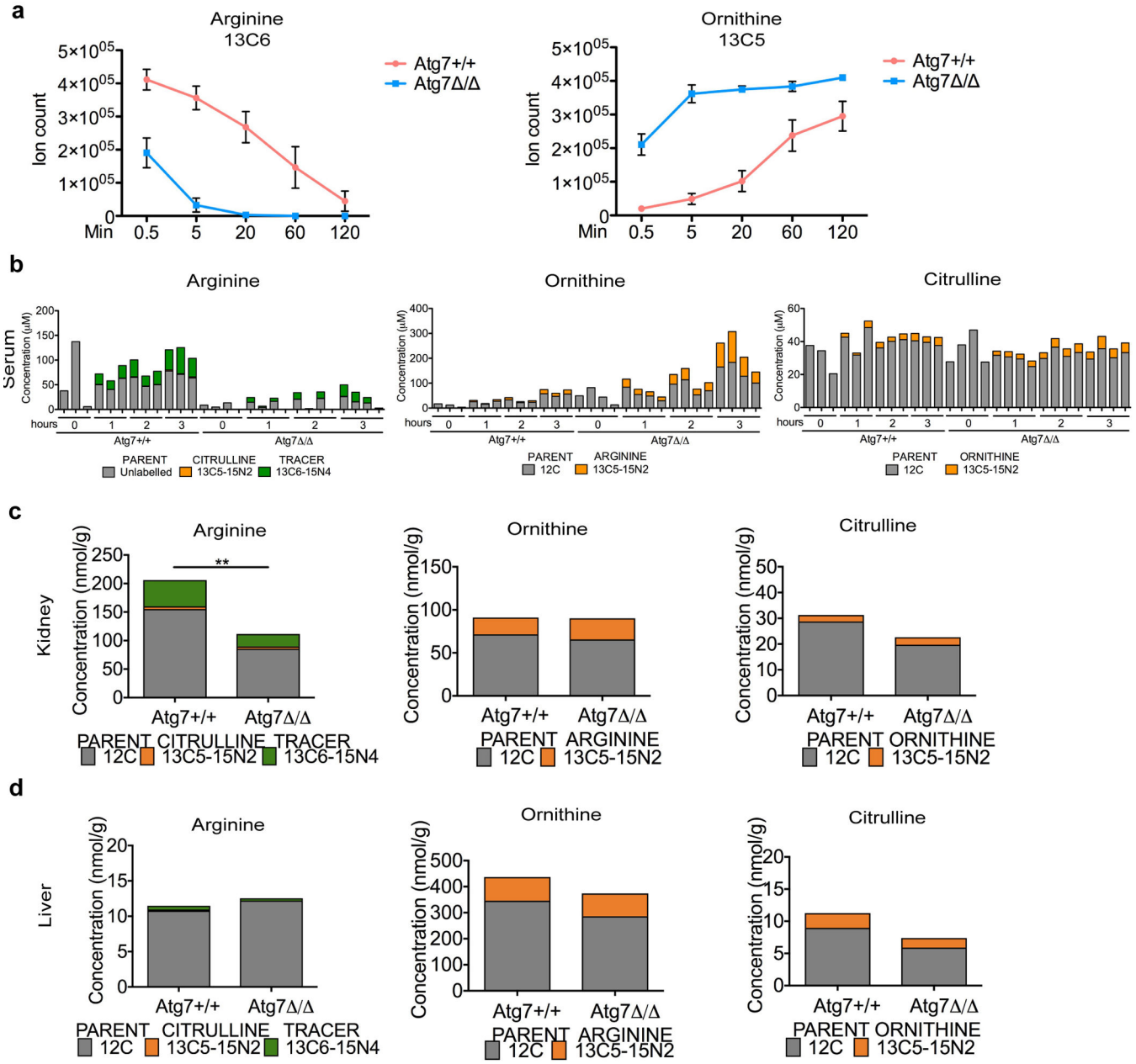

Extended data Fig. 4: *Atg7* deletion increases serum arginine degradation but does not modify arginine metabolism in kidney and liver.

a, Serum $^{13}C_6$-arginine and $^{13}C_5$-ornithine in *Atg7*$^{+/+}$ and *Atg7*$^{\Delta/\Delta}$ hosts (n=3 each) overtime. Data are mean +/− S.E.M. **b,** Concentration (μM) of arginine, citrulline, and ornithine in serum from *Atg7*$^{+/+}$ (n=3) and *Atg7*$^{\Delta/\Delta}$ hosts (n=4) after infusion with $^{13}C_6{}^{15}N_4$-arginine. **c-d,** Concentration (nmol/g) of arginine, citrulline, and ornithine in kidney **(c)** and liver **(d)** from *Atg7*$^{+/+}$ and *Atg7*$^{\Delta/\Delta}$ hosts (n=2 each) after infusion with $^{13}C_6{}^{15}N_4$-arginine. Data are mean (**p<0.01 by Two-way ANOVA test).

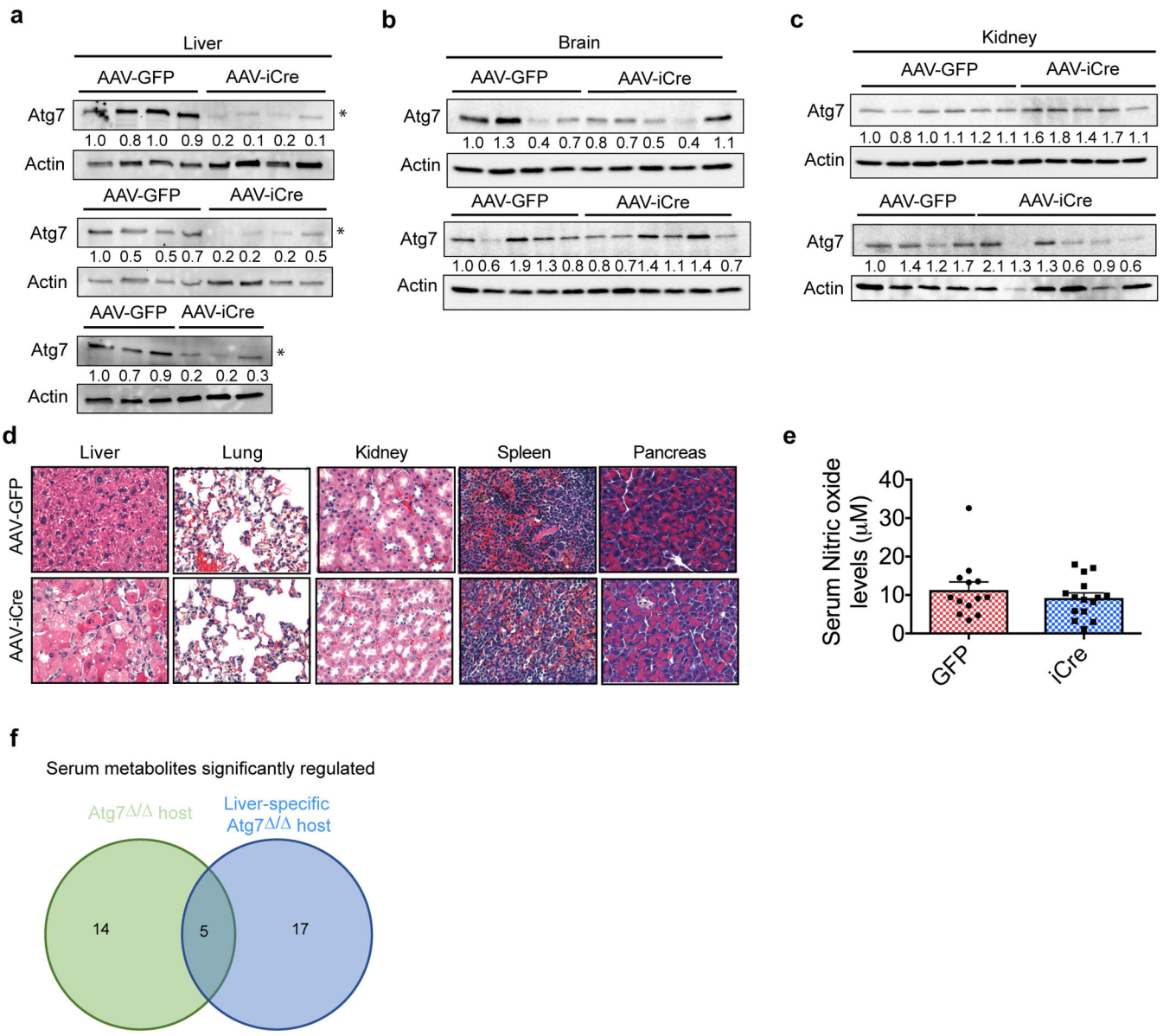

Extended data Fig. 5: Liver-specific *Atg7* deletion lead to liver cell enlargement without affecting other tissues.

a-b-c, Western blotting showing expression of *Atg7* in liver (n=11 each) **(a)**, brain (n= 9 and 11, respectively) **(b)** and kidney (n=10 each) **(c)** from $Atg7^{+/+}$ and liver-specific $Atg7^{\Delta/\Delta}$ hosts. *p<0.05 compared to $Atg7^{+/+}$ hosts. Data are representative of 2 independent experiments. Actin was used as a loading control. **d,** Representative H&E tissue staining from $Atg7^{+/+}$ and liver-specific $Atg7^{\Delta/\Delta}$ hosts. Pictures are representative of 2 independent experiments. **e,** Analysis of serum nitric oxide levels in $Atg7^{+/+}$(n=13) and liver-specific $Atg7^{\Delta/\Delta}$ (n=15) hosts. Data are mean +/− S.E.M. **f,** Comparison of serum metabolites significantly regulated in $Atg7^{\Delta/\Delta}$ and liver-specific $Atg7^{\Delta/\Delta}$ hosts (n=17 each, p<0.05).

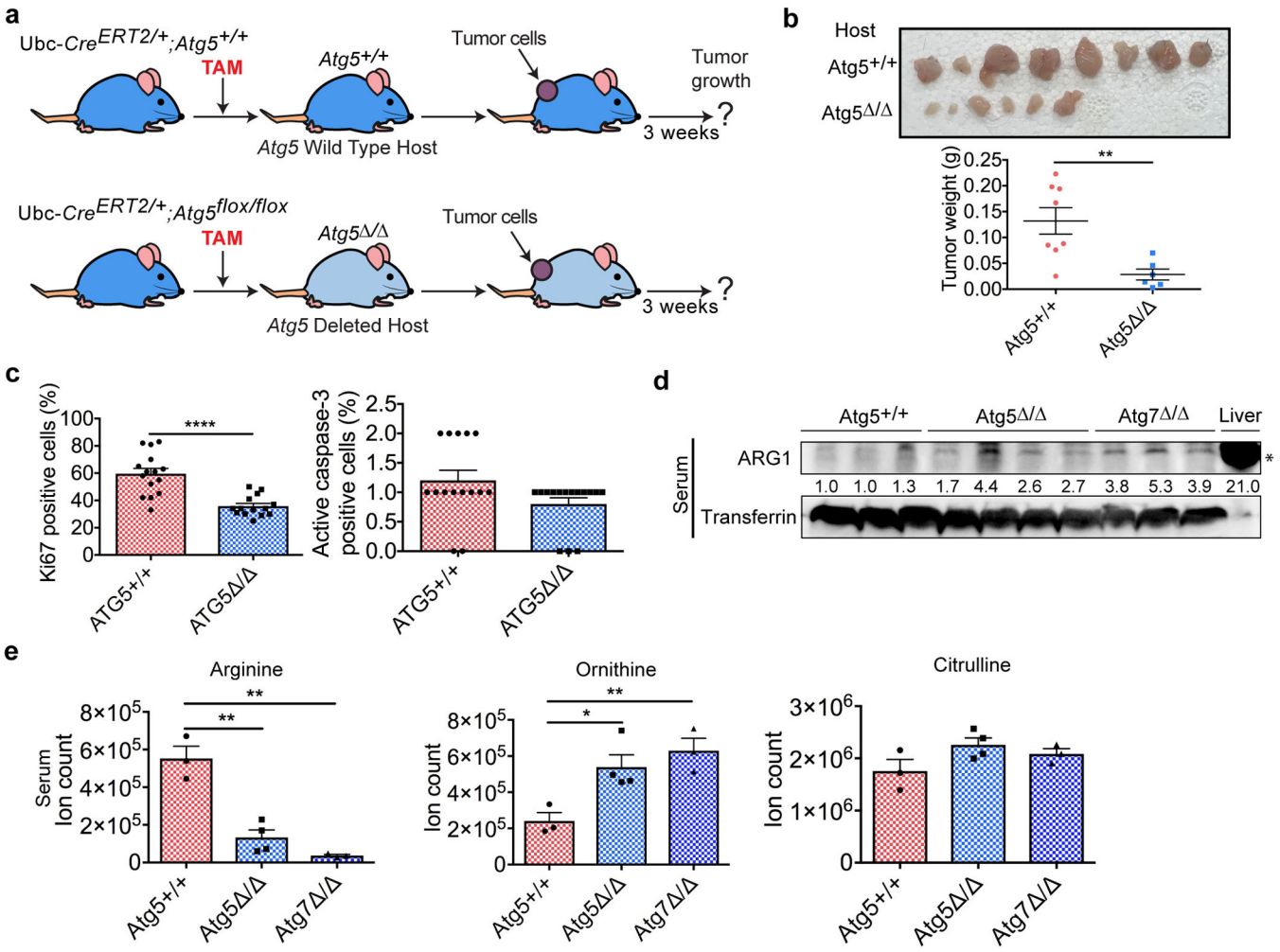

Extended data Fig. 6: *Atg5* deletion increased serum ARG1, decreased serum arginine and tumor growth.

a, Experimental design to induce host mice with conditional whole-body *Atg5* deletion ($Atg5^{\Delta/\Delta}$) and wild type controls ($Atg5^{+/+}$) with which to assess tumor growth. Ubc-$Cre^{ERT2/+}$;$Atg5^{+/+}$ and Ubc-$Cre^{ERT2/+}$;$Atg5^{flox/flox}$ mice were injected with TAM at 8 to 10 weeks of age to delete *Atg5* and create $Atg5^{+/+}$ and $Atg5^{\Delta/\Delta}$ hosts. Mice were then injected subcutaneously with tumor cells and tumor growth was monitored over 3 weeks. **b,** Comparison of tumor weight between $Atg5^{+/+}$ (n=4) and $Atg5^{\Delta/\Delta}$ hosts (n=3). Data are mean +/− S.E.M (**p<0.01). **c,** IHC quantification of Ki67 and active Caspase-3 positive cells in tumors from $Atg5^{+/+}$ and $Atg5^{\Delta/\Delta}$ hosts. Data are mean +/− S.E.M (****p<0.0001). **d,** Western blotting showing expression of ARG1 in serum from $Atg5^{+/+}$ (n=3), $Atg5^{\Delta/\Delta}$ (n=4) and $Atg7^{\Delta/\Delta}$ (n=3) hosts. *p<0.05 compared to $Atg5^{+/+}$ hosts. Transferrin was used as a loading control **e,** Serum arginine, ornithine and citrulline levels in $Atg5^{+/+}$ (n=4) and $Atg5^{\Delta/\Delta}$ (n=3) hosts obtained by LC-MS. Data are mean +/− S.E.M (*p<0.05, **p<0.01).

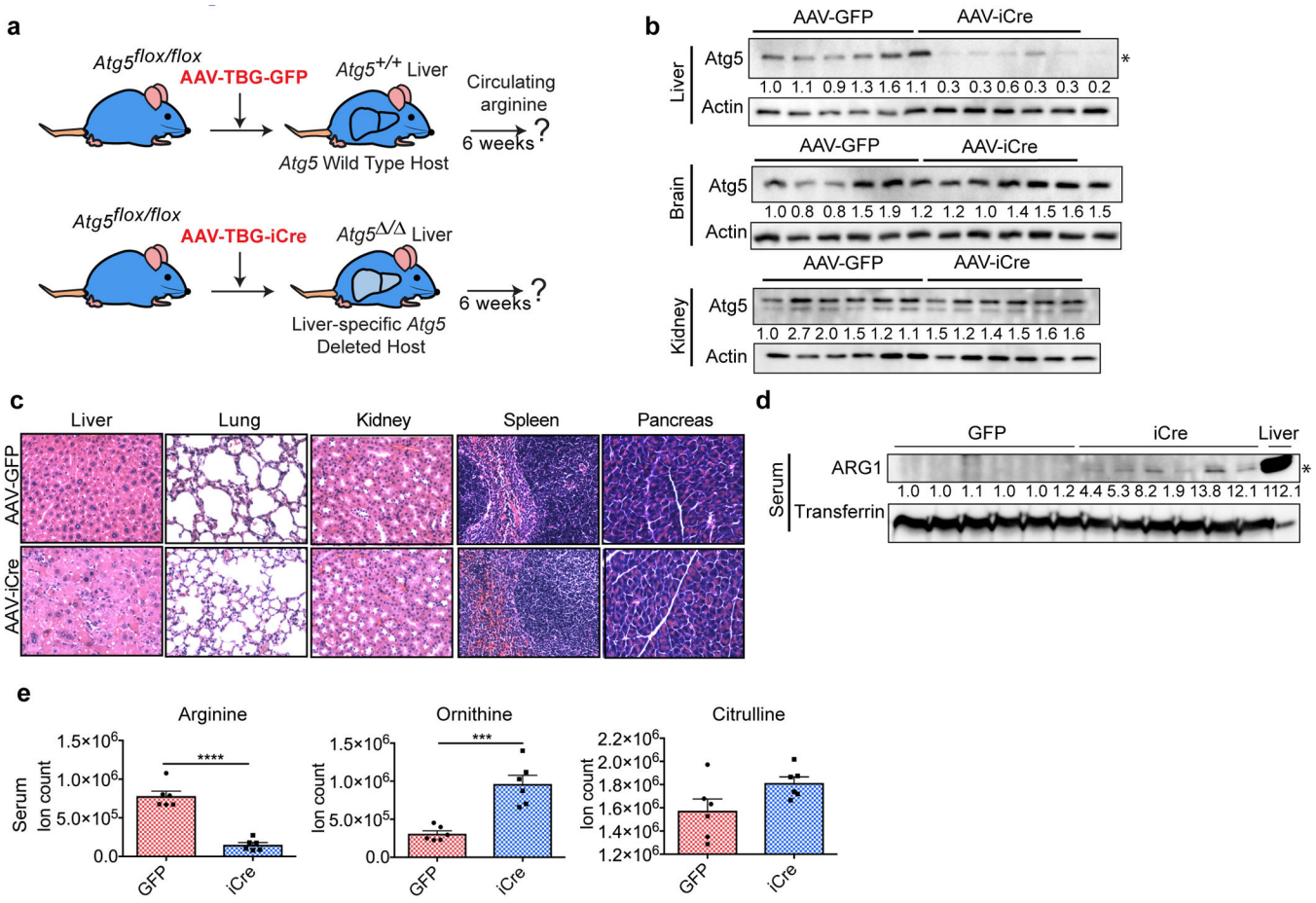

Extended data Fig. 7: Liver-specific *Atg5* deleted hosts present liver cell enlargement, increased serum ARG1 and decreased serum arginine.

a, Experimental design to induce liver-specific deletion of *Atg5*. *Atg5*$^{flox/flox}$ mice were injected (tail vein) with AAV-TBG-GFP or AAV-TBG-iCre at 8 to 10 weeks of age to delete *Atg5* in liver and create *Atg5*$^{+/+}$ and liver-specific *Atg5*$^{\Delta/\Delta}$ hosts, respectively. **b,** Western blotting showing expression of *Atg5* in liver, brain and kidney from *Atg5*$^{+/+}$ and liver-specific *Atg5*$^{\Delta/\Delta}$ hosts (n=6 each). *p<0.05 compared to *Atg5*$^{+/+}$ hosts. Actin was used as a loading control **c,** H&E tissue staining from *Atg5*$^{+/+}$ and liver-specific *Atg5*$^{\Delta/\Delta}$ hosts (n=6 each). **d,** Western blotting showing expression of ARG1 in serum from *Atg5*$^{+/+}$ and liver-specific *Atg5*$^{\Delta/\Delta}$ hosts (n=6 each). *p<0.05 compared to *Atg5*$^{+/+}$ hosts. Transferrin was used as a loading control **e,** Serum arginine, ornithine and citrulline levels in *Atg5*$^{+/+}$ and liver-specific *Atg5*$^{\Delta/\Delta}$ hosts (n=6 each) obtained by LC-MS. Data are mean +/− S.E.M (***p<0.001, ****p<0.0001).

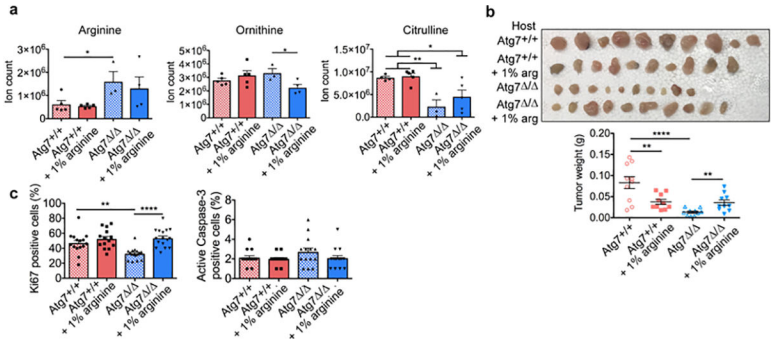

Extended data Fig. 8: Dietary arginine supplementation rescues YUMM 1.3 tumor growth in *Atg7*$^{\Delta/\Delta}$ hosts.

a, Serum arginine, ornithine and citrulline in *Atg7*$^{+/+}$ (n=5), *Atg7*$^{+/+}$ + 1% arg (n=5), *Atg7*$^{\Delta/\Delta}$ (n=6) and *Atg7*$^{\Delta/\Delta}$ + 1% arg (n=6) hosts, obtained by LC-MS. Data are mean +/− S.E.M (*p<0.05, **p<0.01). **b,** Comparison of YUMM 1.3 tumor weight between *Atg7*$^{+/+}$ and *Atg7*$^{\Delta/\Delta}$ (n=5 each) hosts with or without arginine supplementation. Data are mean +/− S.E.M. (**p<0.01, ****p<0.0001). **c,** IHC quantification of Ki67 and active Caspase-3 positive cells in tumors from *Atg7*$^{+/+}$ and *Atg7*$^{\Delta/\Delta}$ hosts with or without arginine supplementation. Data are mean +/− S.E.M (**p<0.01, ****p<0.0001).

Supplementary Material

Refer to Web version on PubMed Central for supplementary material.

Acknowledgements

This work was supported by National Institutes of Health grants: R01CA130893, R01CA193970 (to EW), R01CA163591 (to EW and JDR), K22CA190521 (to JYG), R50CA211437 (to WL), R01CA193970 (to JMM), P30CA072720 (Rutgers Cancer Center), and S10OD016400 (Rutgers Biological Mass Spectrometry Facility), and the V Foundation for Cancer Research (to JMM). Laura Poillet-Perez received support from a postdoctoral fellowship from the New Jersey Commission for Cancer Research (DHFS16PPC034). We thank the Rutgers Cancer Institute Metabolomics Service Shared Resource, the Rutgers-New Brunswick/Robert Wood Johnson Medical School Biological Mass Spectrometry Facility for mass spectrometry analysis and Dirk Moore for the statistical analysis of the proteomics data. Illustrations used in Fig. 4e are licensed under the Creative Commons Attribution 3.0 Unported License. To view a copy of this license, visit http://creativecommons.org/licenses/by/3.0/ or send a letter to Creative Commons, PO Box 1866, Mountain View, CA 94042, USA.

References

1. Karsli-Uzunbas G et al. Autophagy is required for glucose homeostasis and lung tumor maintenance. Cancer Discov 4, 914–927, doi:10.1158/2159-8290.CD-14-0363 (2014). [PubMed: 24875857]
2. Komatsu M et al. Impairment of starvation-induced and constitutive autophagy in Atg7-deficient mice. J Cell Biol 169, 425–434, doi:10.1083/jcb.200412022 (2005). [PubMed: 15866887]
3. Kuma A et al. The role of autophagy during the early neonatal starvation period. Nature 432, 1032–1036, doi:10.1038/nature03029 (2004). [PubMed: 15525940]
4. Guo JY et al. Autophagy provides metabolic substrates to maintain energy charge and nucleotide pools in Ras-driven lung cancer cells. Genes Dev 30, 1704–1717, doi:10.1101/gad.283416.116 (2016). [PubMed: 27516533]
5. Kamada Y, Sekito T & Ohsumi Y Autophagy in yeast: a TOR-mediated response to nutrient starvation. Curr Top Microbiol Immunol 279, 73–84 (2004). [PubMed: 14560952]

6. Kimmelman AC & White E Autophagy and Tumor Metabolism. Cell Metab 25, 1037–1043, doi: 10.1016/j.cmet.2017.04.004 (2017). [PubMed: 28467923]
7. Amaravadi R, Kimmelman AC & White E Recent insights into the function of autophagy in cancer. Genes Dev 30, 1913–1930, doi:10.1101/gad.287524.116 (2016). [PubMed: 27664235]
8. Yang A et al. Autophagy Sustains Pancreatic Cancer Growth through Both Cell-Autonomous and Nonautonomous Mechanisms. Cancer Discov, doi:10.1158/2159-8290.CD-17-0952 (2018).
9. Wang J et al. UV-induced somatic mutations elicit a functional T cell response in the YUMMER1.7 mouse melanoma model. Pigment Cell Melanoma Res 30, 428–435, doi:10.1111/pcmr.12591 (2017). [PubMed: 28379630]
10. Strohecker AM et al. Autophagy sustains mitochondrial glutamine metabolism and growth of BrafV600E-driven lung tumors. Cancer Discov 3, 1272–1285, doi: 10.1158/2159-8290.CD-13-0397 (2013). [PubMed: 23965987]
11. Guo JY et al. Autophagy suppresses progression of K-ras-induced lung tumors to oncocytomas and maintains lipid homeostasis. Genes Dev 27, 1447–1461, doi:10.1101/gad.219642.113 (2013). [PubMed: 23824538]
12. Chantranupong L et al. The CASTOR Proteins Are Arginine Sensors for the mTORC1 Pathway. Cell 165, 153–164, doi:10.1016/j.cell.2016.02.035 (2016). [PubMed: 26972053]
13. Morris SM, Jr. Arginine metabolism: boundaries of our knowledge. J Nutr 137, 1602S–1609S (2007). [PubMed: 17513435]
14. Delage B et al. Arginine deprivation and argininosuccinate synthetase expression in the treatment of cancer. Int J Cancer 126, 2762–2772, doi:10.1002/ijc.25202 (2010). [PubMed: 20104527]
15. Dillon BJ et al. Incidence and distribution of argininosuccinate synthetase deficiency in human cancers: a method for identifying cancers sensitive to arginine deprivation. Cancer 100, 826–833, doi:10.1002/cncr.20057 (2004). [PubMed: 14770441]
16. Patil MD, Bhaumik J, Babykutty S, Banerjee UC & Fukumura D Arginine dependence of tumor cells: targeting a chink in cancer's armor. Oncogene 35, 4957–4972, doi:10.1038/onc.2016.37 (2016). [PubMed: 27109103]
17. Rabinovich S et al. Diversion of aspartate in ASS1-deficient tumours fosters de novo pyrimidine synthesis. Nature 527, 379–383, doi:10.1038/nature15529 (2015). [PubMed: 26560030]
18. Nagamani SC & Erez A A metabolic link between the urea cycle and cancer cell proliferation. Mol Cell Oncol 3, e1127314, doi:10.1080/23723556.2015.1127314 (2016). [PubMed: 27308634]
19. Feun LG et al. Negative argininosuccinate synthetase expression in melanoma tumours may predict clinical benefit from arginine-depleting therapy with pegylated arginine deiminase. Br J Cancer 106, 1481–1485, doi:10.1038/bjc.2012.106 (2012). [PubMed: 22472884]
20. Lam TL et al. Recombinant human arginase inhibits the in vitro and in vivo proliferation of human melanoma by inducing cell cycle arrest and apoptosis. Pigment Cell Melanoma Res 24, 366–376, doi:10.1111/j.1755-148X.2010.00798.x (2011). [PubMed: 21029397]
21. Hui S et al. Glucose feeds the TCA cycle via circulating lactate. Nature 551, 115–118, doi: 10.1038/nature24057 (2017). [PubMed: 29045397]
22. Morris SM, Jr. Arginases and arginine deficiency syndromes. Curr Opin Clin Nutr Metab Care 15, 64–70, doi:10.1097/MCO.0b013e32834d1a08 (2012). [PubMed: 22037011]
23. Takamura A et al. Autophagy-deficient mice develop multiple liver tumors. Genes Dev 25, 795–800, doi:10.1101/gad.2016211 (2011). [PubMed: 21498569]
24. Komatsu M et al. Homeostatic levels of p62 control cytoplasmic inclusion body formation in autophagy-deficient mice. Cell 131, 1149–1163, doi:10.1016/j.cell.2007.10.035 (2007). [PubMed: 18083104]
25. Sousa CM et al. Pancreatic stellate cells support tumour metabolism through autophagic alanine secretion. Nature 536, 479–483, doi:10.1038/nature19084 (2016). [PubMed: 27509858]
26. Katheder NS et al. Microenvironmental autophagy promotes tumour growth. Nature 541, 417–420, doi:10.1038/nature20815 (2017). [PubMed: 28077876]
27. Kremer JC et al. Arginine Deprivation Inhibits the Warburg Effect and Upregulates Glutamine Anaplerosis and Serine Biosynthesis in ASS1-Deficient Cancers. Cell Rep 18, 991–1004, doi: 10.1016/j.celrep.2016.12.077 (2017). [PubMed: 28122247]

28. Yau T et al. A phase 1 dose-escalating study of pegylated recombinant human arginase 1 (Peg-rhArg1) in patients with advanced hepatocellular carcinoma. Invest New Drugs 31, 99–107, doi: 10.1007/s10637-012-9807-9 (2013). [PubMed: 22426640]
29. Shen W et al. A novel and promising therapeutic approach for NSCLC: recombinant human arginase alone or combined with autophagy inhibitor. Cell Death Dis 8, e2720, doi:10.1038/cddis. 2017.137 (2017). [PubMed: 28358368]
30. Koprivnikar J, McCloskey J & Faderl S Safety, efficacy, and clinical utility of asparaginase in the treatment of adult patients with acute lymphoblastic leukemia. Onco Targets Ther 10, 1413–1422, doi:10.2147/OTT.S106810 (2017). [PubMed: 28331334]
31. Ruzankina Y et al. Deletion of the developmentally essential gene ATR in adult mice leads to age-related phenotypes and stem cell loss. Cell Stem Cell 1, 113–126, doi:10.1016/j.stem.2007.03.002 (2007). [PubMed: 18371340]
32. Hara T et al. Suppression of basal autophagy in neural cells causes neurodegenerative disease in mice. Nature 441, 885–889, doi:10.1038/nature04724 (2006). [PubMed: 16625204]
33. Meeth K, Wang JX, Micevic G, Damsky W & Bosenberg MW The YUMM lines: a series of congenic mouse melanoma cell lines with defined genetic alterations. Pigment Cell Melanoma Res 29, 590–597, doi:10.1111/pcmr.12498 (2016). [PubMed: 27287723]
34. Summerhayes IC & Franks LM Effects of donor age on neoplastic transformation of adult mouse bladder epithelium in vitro. J Natl Cancer Inst 62, 1017–1023 (1979). [PubMed: 107359]
35. Lu W et al. Metabolomic analysis via reversed-phase ion-pairing liquid chromatography coupled to a stand alone orbitrap mass spectrometer. Anal Chem 82, 3212–3221, doi:10.1021/ac902837x (2010). [PubMed: 20349993]
36. Papazyan R et al. Physiological Suppression of Lipotoxic Liver Damage by Complementary Actions of HDAC3 and SCAP/SREBP. Cell Metab 24, 863–874, doi:10.1016/j.cmet.2016.10.012 (2016). [PubMed: 27866836]
37. Melamud E, Vastag L & Rabinowitz JD Metabolomic analysis and visualization engine for LC-MS data. Anal Chem 82, 9818–9826, doi:10.1021/ac1021166 (2010). [PubMed: 21049934]
38. Zhan L et al. Dysregulation of bile acid homeostasis in parenteral nutrition mouse model. Am J Physiol Gastrointest Liver Physiol 310, G93–G102, doi:10.1152/ajpgi.00252.2015 (2016). [PubMed: 26564717]
39. Su X, Lu W & Rabinowitz JD Metabolite Spectral Accuracy on Orbitraps. Anal Chem 89, 5940–5948, doi:10.1021/acs.analchem.7b00396 (2017). [PubMed: 28471646]
40. Sailer M et al. Increased plasma citrulline in mice marks diet-induced obesity and may predict the development of the metabolic syndrome. PLoS One 8, e63950, doi:10.1371/journal.pone.0063950 (2013). [PubMed: 23691124]
41. Sleat DE et al. Mass spectrometry-based protein profiling to determine the cause of lysosomal storage diseases of unknown etiology. Mol Cell Proteomics 8, 1708–1718, doi:10.1074/ mcp.M900122-MCP200 (2009). [PubMed: 19383612]
42. Beavis RC Using the global proteome machine for protein identification. Methods Mol Biol 328, 217–228, doi:10.1385/1-59745-026-X:217 (2006). [PubMed: 16785652]
43. Lund SP, Nettleton D, McCarthy DJ & Smyth GK Detecting differential expression in RNA-sequence data using quasi-likelihood with shrunken dispersion estimates. Stat Appl Genet Mol Biol 11, doi:10.1515/1544-6115.1826 (2012).

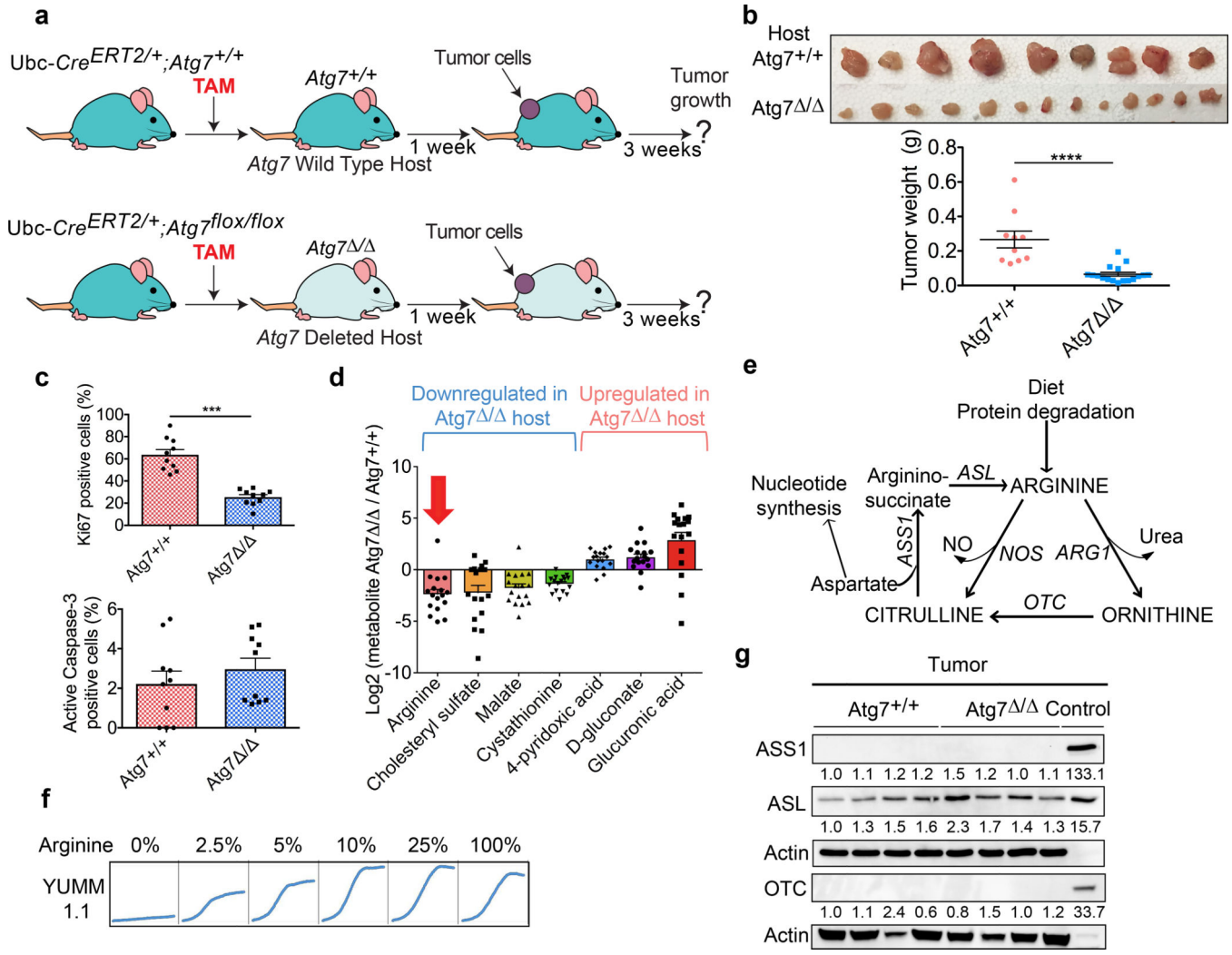

Fig. 1: Host autophagy promotes growth of arginine auxotrophic tumors.

a, Experimental design to induce host mice with conditional whole-body *Atg7* deletion (*Atg7*$^{\Delta/\Delta}$) and wild type controls (*Atg7*$^{+/+}$) with which to assess tumor growth. Ubc-*Cre*$^{ERT2/+}$;*Atg7*$^{+/+}$ and Ubc-*Cre*$^{ERT2/+}$;*Atg7*$^{flox/flox}$ mice were injected with TAM to delete *Atg7* and were then injected subcutaneously with tumor cells. Tumor growth was monitored over 3 weeks. **b,** Comparison of tumor weight between *Atg7*$^{+/+}$ (n=5) and *Atg7*$^{\Delta/\Delta}$ hosts (n=8). Data are mean +/− S.E.M (****p<0.0001). **c,** IHC quantification of Ki67 and active Caspase-3 positive cells in tumors from *Atg7*$^{+/+}$ and *Atg7*$^{\Delta/\Delta}$ hosts. Data are mean +/− S.E.M (***p<0.001). **d,** Serum metabolites with log2 fold change cut-offs of >1 or <−1 between *Atg7*$^{+/+}$ (n=17) and *Atg7*$^{\Delta/\Delta}$ (n=17) hosts obtained by LC-MS with p<0.05. **e,** Illustration of the arginine metabolism. ASS1, Argininosuccinate synthase 1; ASL, Argininosuccinate lyase; ARG1, Arginase 1; NOS, Nitric oxide synthetase; OTC, Ornithine transcarbamylase. **f,** YUMM 1.1 proliferation *in vitro* in medium containing different percentages of arginine. Cell density was measured every 2 hours using IncuCyte. Data are representative of 3 independent experiments performed in duplicate. **g,** Western blotting showing expression of ASS1, ASL and OTC in tumors from *Atg7*$^{+/+}$ and *Atg7*$^{\Delta/\Delta}$ hosts (n=4

each) representative of 3 independent experiments. Kidney was used as a control tissue for ASS1 and ASL while liver was used for OTC. Actin was used a loading control. In all figures, n= number of mice.

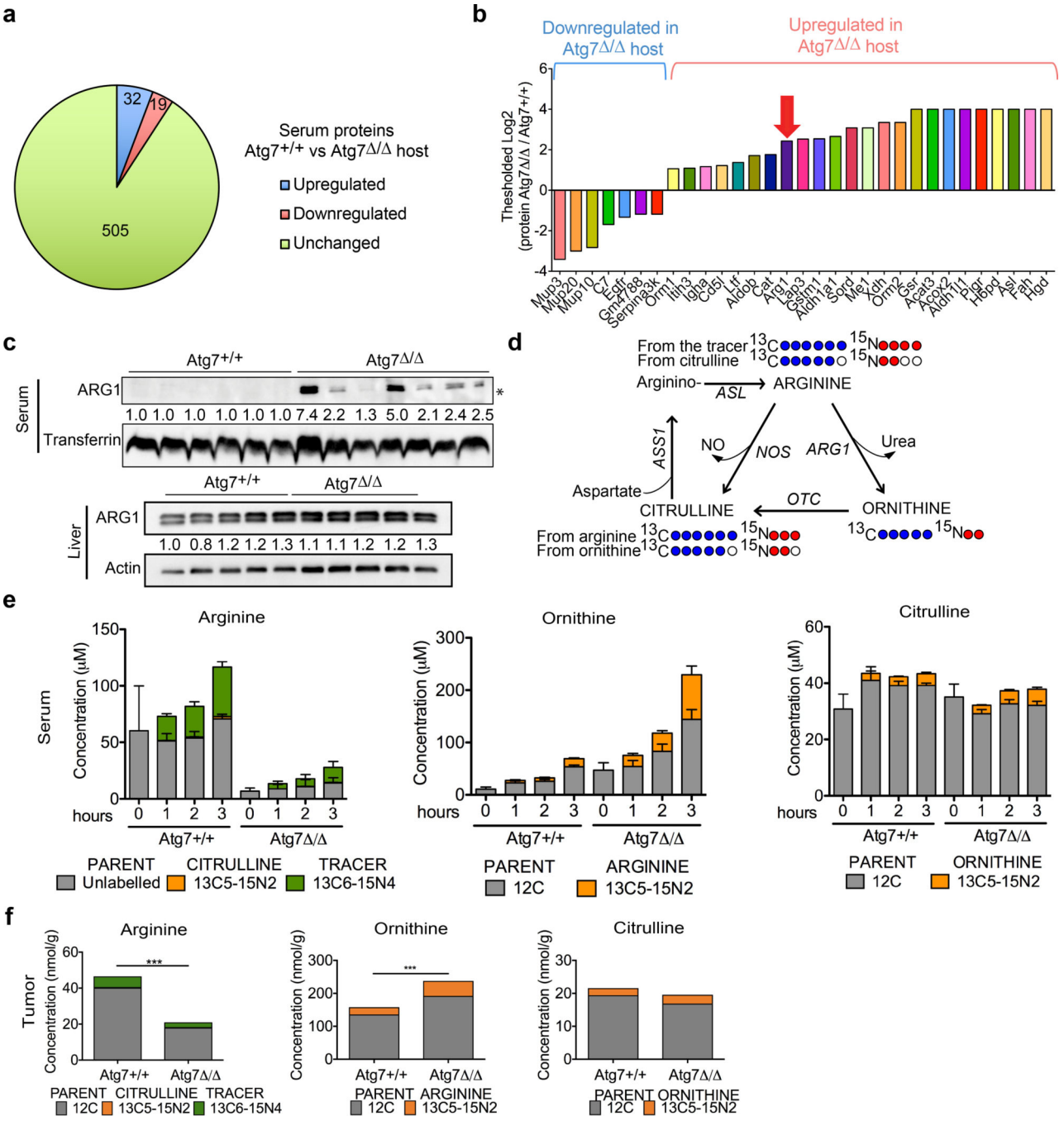

Fig. 2: Serum ARG1 levels increase in *Atg7*$^{\Delta/\Delta}$ hosts and deplete circulating arginine.

a, Comparison of serum proteins between *Atg7*$^{+/+}$ and *Atg7*$^{\Delta/\Delta}$ hosts (n=5 each) obtained by nano LC-MS/MS with corrected p<0.05. **b,** Proteins with log2 fold change cut-offs of >1 or <−1 between *Atg7*$^{+/+}$ and *Atg7*$^{\Delta/\Delta}$ hosts. **c,** Western blotting showing expression of ARG1 in serum and liver from *Atg7*$^{+/+}$ and *Atg7*$^{\Delta/\Delta}$ hosts. *p<0.05 compared to *Atg7*$^{+/+}$ hosts. Data are representative of 2 independent experiments. Actin and transferrin were used as loading controls. **d,** Illustration of the $^{13}C_6{}^{15}N_4$-arginine tracer labelling pattern. **e,** Concentration (μM) of arginine, citrulline, and ornithine in serum from *Atg7*$^{+/+}$ and *Atg7*$^{\Delta/\Delta}$ hosts (n=3 and

4, respectively) after infusion with $^{13}C_6{}^{15}N_4$-arginine. Data are mean +/− S.E.M. **f,** Concentration (nmol/g) of arginine, citrulline, and ornithine in tumor from $Atg7^{+/+}$ and $Atg7^{\Delta/\Delta}$ hosts (n=2 each) after infusion with $^{13}C_6{}^{15}N_4$-arginine. Data are mean (***p<0.001 by Two-way ANOVA test).

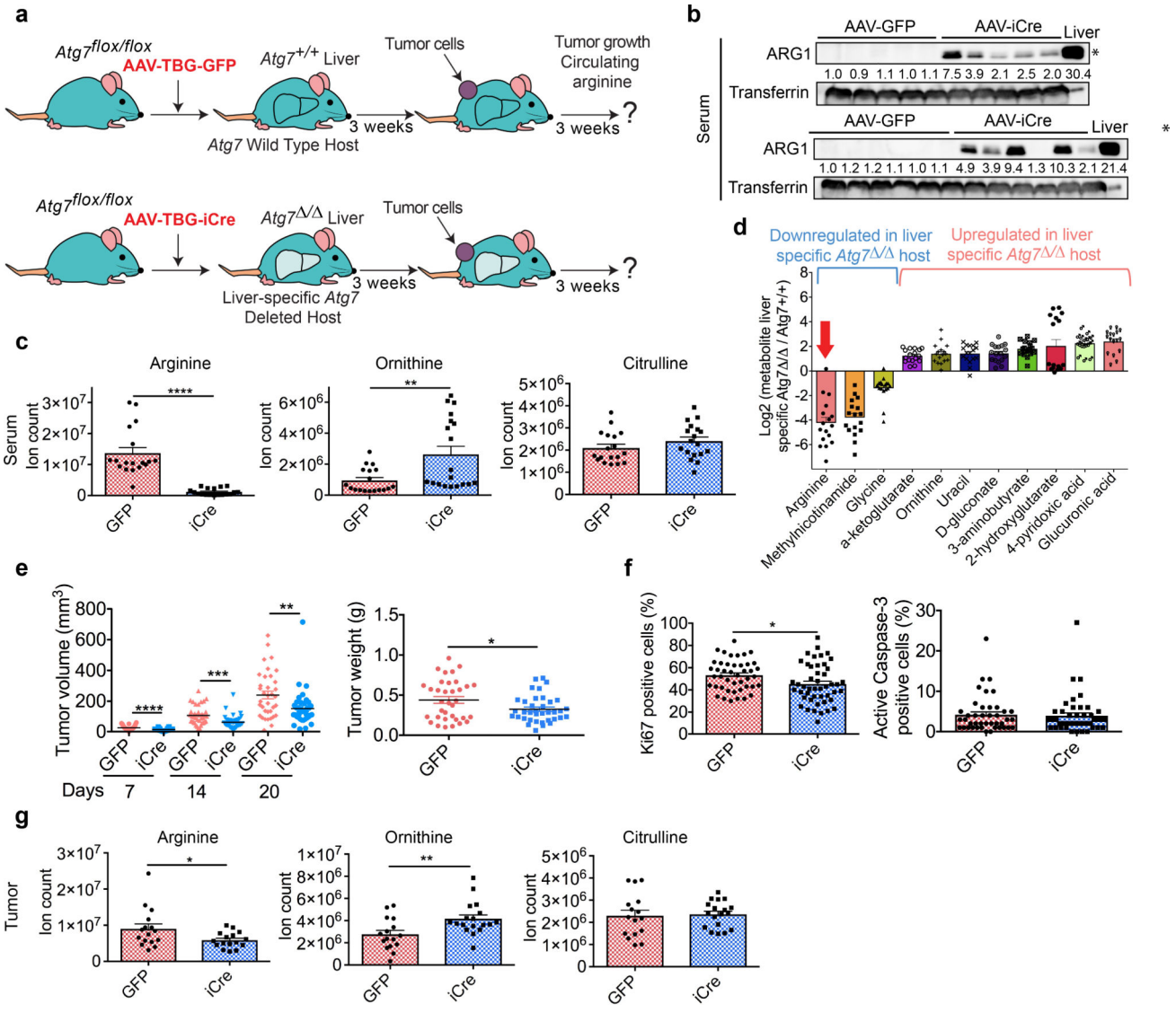

Fig. 3: *Atg7* deletion in liver increases serum ARG1, and decreases serum arginine and tumor growth.

a, Experimental design to induce liver-specific deletion of *Atg7*. $Atg7^{flox/flox}$ mice were injected (tail vein) with AAV-TBG-GFP or AAV-TBG-iCre to delete *Atg7* in liver and were injected subcutaneously with tumor cells. Tumor growth was monitored over 3 weeks. **b,** Western blotting showing expression of ARG1 in serum from $Atg7^{+/+}$ and liver-specific $Atg7^{\Delta/\Delta}$ hosts (n=11 each). *p<0.05 compared to $Atg7^{+/+}$ hosts. Data are representative of 2 independent experiments. Transferrin was used as a loading control. **c,** Serum arginine, ornithine and citrulline levels in $Atg7^{+/+}$ and liver-specific $Atg7^{\Delta/\Delta}$ hosts (n=18 each) obtained by LC-MS. Data are mean +/− S.E.M (**p<0.01, ****p<0.0001). **d,** Serum metabolites with log2 fold change cut-offs of >1 or <−1 between $Atg7^{+/+}$ and liver-specific $Atg7^{\Delta/\Delta}$ hosts (n=17 each) obtained by LC-MS with p<0.05. Data are mean +/− S.E.M. **e,** Comparison of tumor volume and weight between $Atg7^{+/+}$ (n=17) and liver-specific $Atg7^{\Delta/\Delta}$ hosts (n=19). Data are mean +/− S.E.M (*p<0.05, **p<0.01, ***p<0.001, ****p<0.0001). **f,** IHC quantification of Ki67 and active Caspase-3 positive cells in tumors from $Atg7^{+/+}$ and

liver-specific $Atg7^{\Delta/\Delta}$ hosts. Data are mean +/− S.E.M (*p<0.05). **g,** Tumor arginine, ornithine and citrulline levels in $Atg7^{+/+}$ (n=16) and liver-specific $Atg7^{\Delta/\Delta}$ (n=16) hosts obtained by LC-MS. Data are mean +/− S.E.M (*p<0.05, **p<0.01).

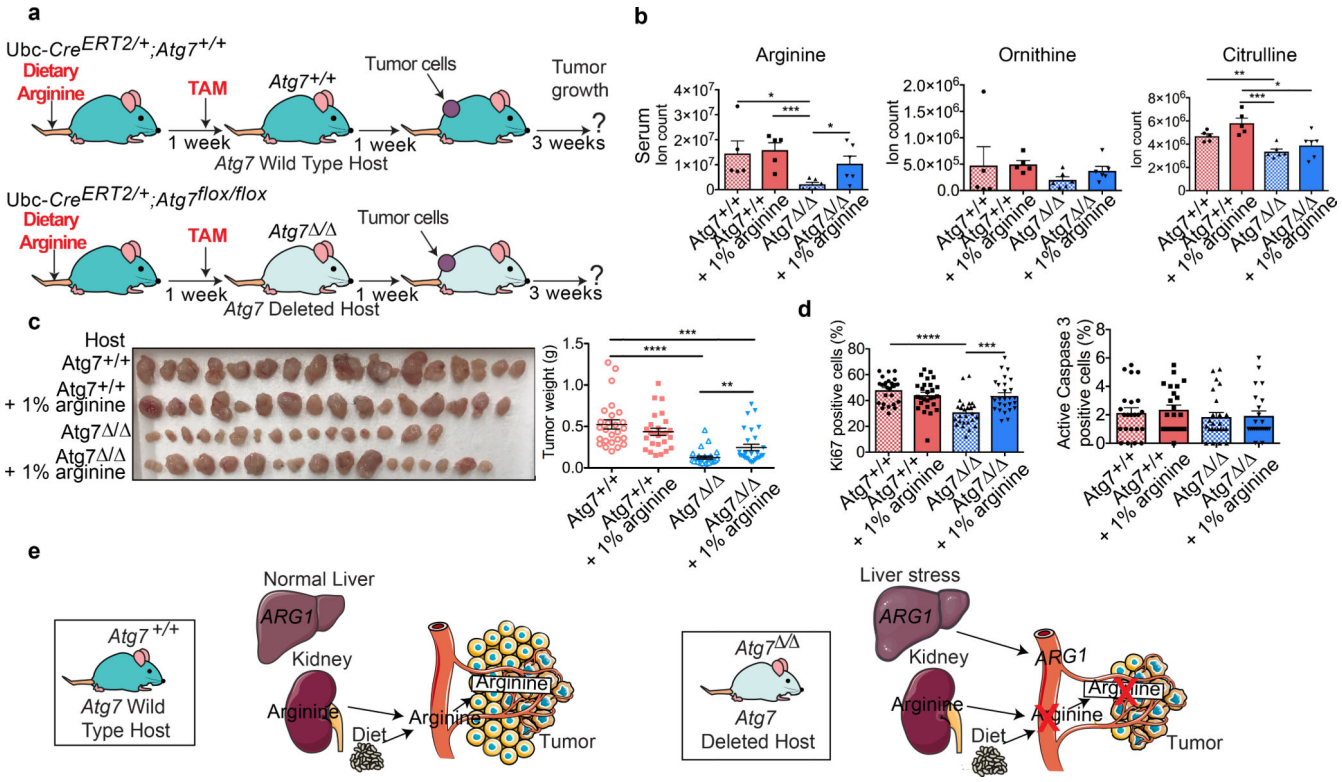

Fig. 4: Dietary arginine supplementation rescues tumor growth in *Atg7*$^{\Delta/\Delta}$ hosts.

a, Experimental design to perform arginine supplementation and induce conditional whole-body *Atg7* deletion to assess YUMM 1.1 tumor growth. Ubc-*Cre*$^{ERT2/+}$;*Atg7*$^{+/+}$ and Ubc-*Cre*$^{ERT2/+}$;*Atg7*$^{flox/flox}$ mice were supplied with supplementary dietary arginine (0 or 1%). Seven days later, TAM was injected to delete *Atg7* and mice were injected subcutaneously with tumor cells. Tumor growth was monitored over 3 weeks. **b,** Serum arginine, ornithine and citrulline in *Atg7*$^{+/+}$ (n=5) and *Atg7*$^{\Delta/\Delta}$ (n=6) hosts with or without arginine supplementation, obtained by LC-MS. Data are mean +/− S.E.M (*p<0.05, **p<0.01, ***p<0.001). **c,** Comparison of tumor weight between *Atg7*$^{+/+}$ (n=13), *Atg7*$^{+/+}$ + 1% arginine (n=13), *Atg7*$^{\Delta/\Delta}$ (n=13) and *Atg7*$^{\Delta/\Delta}$ + 1% arginine (n=14) hosts. Data are mean +/− S.E.M (**p<0.01, ***p<0.001, ****p<0.0001). **d,** IHC quantification of Ki67 and active Caspase-3 positive cells in tumors from *Atg7*$^{+/+}$ and *Atg7*$^{\Delta/\Delta}$ hosts with or without arginine supplementation. Data are mean +/− S.E.M (***p<0.001, ****p<0.0001). **e,** Model of host autophagy promoting tumor growth.